Investigation of an Innovative Injector for Rotating Detonation Rocket Engines

Ali Hamza

A thesis submitted in partial fulfillment of the requirements for the degree of

Master of Science in Aeronautics and Astronautics

University of Washington 2024

Committee:

Carl Knowlen (Chair)

James Hermanson

Program Authorized to Offer Degree:

William E. Boeing Department of Aeronautics and Astronautics

Investigation of an Innovative Injector for Rotating Detonation Rocket Engines

Chair of the Supervisory Committee:

Dr. Carl Knowlen

Aeronautics and Astronautics

University of Washington

Abstract

A novel injector designed to improve mixing from discrete injector pairs has been investigated with transient, non-reactive, three-dimensional CFD simulations. Subsurface impingement was found to mix gaseous methane and oxygen quicker than above surface impingement. Adding a thin slot to the injector improved both the axial and azimuthal mixing of the gases prior to their injection into the annular combustor of a rotating detonation rocket engine. The slot sizes can be made small enough to prevent detonation waves from propagating upstream and inhibit other types of flashback. The configuration investigated is readily fabricated and easily incorporated into current RDRE rigs being tested at the University of Washington. The results of this CFD study indicate that this injector concept may enable significant improvements in combustion efficiency and pressure gain in RDRE combustors.

TABLE OF CONTENTS

List of Figures

List of Tables

Acknowledgements

The author would like to thank Quentin Roberts for laying the foundation for this project with his groundbreaking work on propellant mixing, and for his substantial assistance with simulation setup and troubleshooting throughout this study. The author also greatly appreciates his research advisor Dr. Carl Knowlen for the opportunity to work in the RDE lab and for continual guidance throughout the MSAA program. He is grateful to Dr. Knowlen, Quentin, and Ty Mundt for their instruction in RDE operation and testing over the 2022-2023 school year.

The author is also indebted to his teachers, who have contributed immensely to his growth as an engineer and encouraged his passion for the mathematical and physical sciences. Among them are Dr. Robert Breidenthal, Dr. Michelle DiBenedetto, Dr. Amin Rahman, Dr. James Hermanson, Dr. Mark Kot, Dr. Baptiste Journaux and Dr. Joshua Krissansen-Totton.

Lastly, the author would like to acknowledge his family and all the friends he has made in Washington. He will always appreciate them for motivating and supporting him through all of his endeavors these past two years.

CHAPTER 1: Introduction

Rotating Detonation Rocket Engines (RDREs) utilize an annular combustion chamber rather than an open cylinder as shown in Fig. 1. This shape allows them to stabilize the rotating detonation waves that form and harness their motion to combust the propellants that are injected at one end of the combustor. These detonation waves travel transversely to the propellant, which is flowing in the axial direction, and therefore rotate around the azimuth. As a result, the injector face is a ring as opposed to a flat circle in a conventional combustor. The performance of a new injector concept and the way it mixes the propellant prior to combustion is a central focus of this thesis.

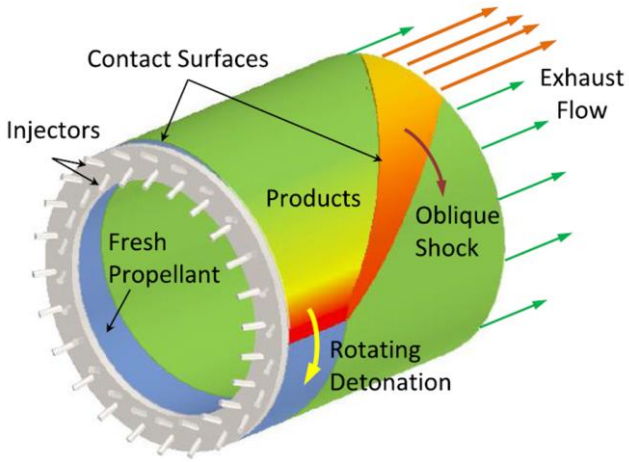

Figure 1.1: Rotating Detonation Combustor diagram [1].

Advantages of rotating detonation engines include increased thermodynamic efficiency over the Brayton cycle due to the higher pressures and temperatures at which combustion occurs, potential pressure gain in the combustor, easier scaling of engine size, and robust operation over a wide range of mixtures. Combustor pressure gain will reduce the required power input from turbomachinery, lowering mass and complexity of the feed system. In addition, the length of the combustion chamber itself is significantly shorter than a conventional one with the same diameter, which makes these engines considerably lighter.

CHAPTER 2: Background

The higher thrust potential and efficiency of detonation engines have yet to be demonstrated for several reasons. Pre-detonation combustion can occur ahead of the detonation zone, which reduces the amount of propellant that can react in the detonation wave. This reduces the amount of heat release behind the wave and thus its pressure rise. Gamba et al. [2] identified this loss mechanism as parasitic deflagration and found that it can also occur at the contact surface between the hot post-combustion gases and the incoming fill mixture. In Fig. 1, this contact surface is represented by the boundary of blue and lime green. Pre-combustion can also be caused by the occurrence of recirculation zones near sharp edges or corners. Recirculation regions are observed in several regions of the flow fields determined by ANSYS simulations, both in this study and in those of past students in the UW RDRE Laboratory [3,4,5].

Engine efficiency and performance directly depend upon the fraction of propellant that reacts completely. Therefore, achieving maximum mixing is crucial and may even be worth implementing design changes that sacrifice pressure gain or increase chamber length (and therefore engine mass). This thesis examines two main factors that influence propellant mixing: the impingement point of the injectants and the use of a thin premixing channel prior to the combustor. The fuel-oxidizer ratio is normalized by computing the equivalence ratio ϕ, which is the quotient of the mass flow ratio of the injected propellants and its stoichiometric ratio [2], defined below in Eq. 1.

$$\phi = \frac{F/O_{actual}}{F/O_{stoich}} = \frac{\dot{m}_f/\dot{m}_{ox}}{F/O_{stoich}} \qquad [1]$$

The mass ratio of CH_4 to O_2 for stoichiometric combustion is 1 to 4, or 0.25. Conventional injector designs typically have the fuel and oxidizer streams impinge after they enter the combustion chamber. This creates fuel-rich and oxidizer-rich zones close to the injector face. In

an effort to mitigate this, Burke et al. [6] experimented with mixing the streams prior to the combustion chamber and found that the inhomogeneities were reduced, creating more uniformly mixed propellant at the start of the chamber. In addition, premixing caused detonation wave speed to increase, as the waves were uninhibited by inhomogeneities in the reactant mixture [6]. However, their method of premixing was bypassing some fuel into the oxidizer in the feed system rather than changing the injector design altogether. In this thesis, four configurations are investigated that impinge the propellant streams at or before the entrance of the detonation annulus as a means to enhance mixing efficiency.

CHAPTER 3: Design and Setup

3.1 Injector Designs

A preliminary design for a subsurface-impinging injector for a 50-mm-diameter by 40-mm-long annular combustor was created in SolidWorks. This is an oxidizer-on-fuel doublet injector with 72 impinging pairs. It was designed to be machined from 360 brass. Parameters of the injector design are provided in Table 3.1. Each doublet impinged at an included angle of 60˚ with the fuel and oxidizer orifices both inclined 30˚ from the central axis. The oxidizer orifice was 1.00 mm in diameter and the fuel orifice was 0.64 mm in diameter, resulting in an oxidizer-to-fuel orifice area ratio of 2.44. The radius from the center of the combustion chamber to the impingement point was 22.5 mm, which corresponds to the center of the 5-mm-wide annular gap combustor configuration. All the fuel orifices were fed from a coaxial annular plenum, and all the oxidizer orifices were fed from a radial plenum, as seen in Fig. 3.1.

Table 3.1: Nook Injector driving dimensions and characteristics

Number of Pairs = 72	Impingement angle = 60˚
Oxidizer d = 1.00 mm	Impingement d = 45 mm
Fuel d = 0.64 mm	Oxidizer/Fuel AR = 2.44
Oxidizer angle from axis = 30˚	Chamber Inner Diameter = 40 mm
Fuel angle from axis = 30˚	Chamber Outer Diameter = 50 mm

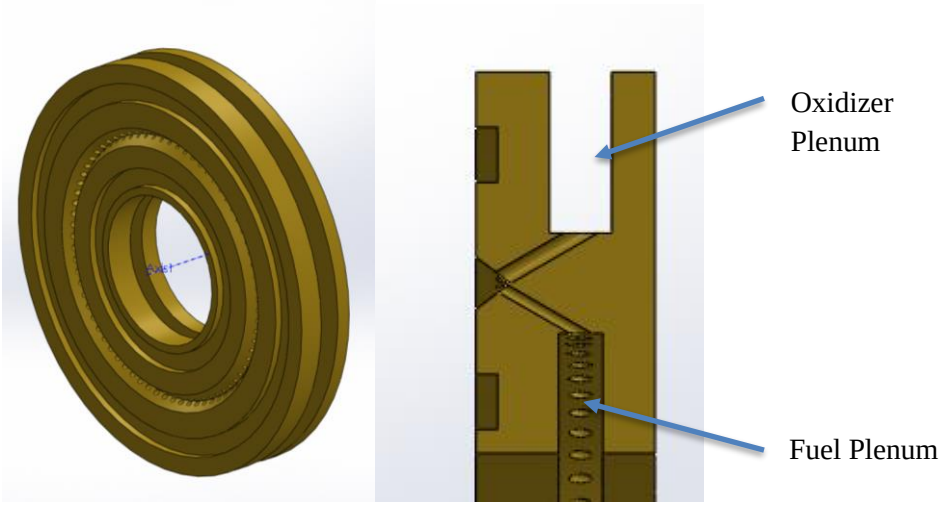

Figure 3.1 CAD Model of Nook Injector, (a) full isometric view, (b) magnified section view.

These injector ports were designed to have their jets impinge below the surface of the injector face. This particular configuration takes advantage of an intermediate fabrication step used in the machining of this kind of impinging injector design. This injector was also designed to be a drop-in replacement for injectors currently being used in the UW RDRE research program. As such, it can be modified with the attachment of two annular extrusions that form a thin annular slot centered around the impingement diameter as shown in Fig. 3.2. The slot lengths considered here were either five or ten slot widths long.

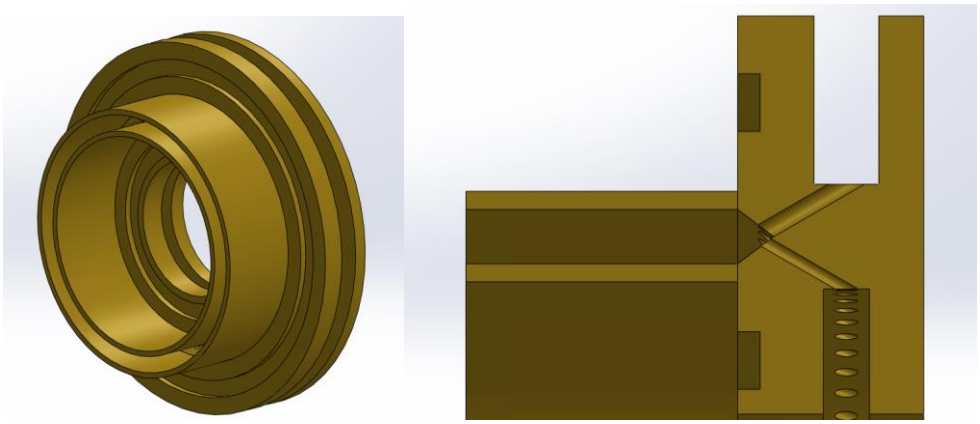

Figure 3.2 CAD Model of Nook Injector with slot extension, (a) full isometric view, (b) magnified section view.

3.2 Flow Domains

The flow domains for all simulations include the fuel and oxidizer plenums, the injector channels, and the annular chamber with a length of 50 mm. Radial symmetry was assumed and 1/72 slice of the full domain is implemented, which corresponds to a single fuel-oxidizer injector pair. To create the remaining domains, the geometry was modified in SolidWorks. The base case removes the slot feature entirely, impinging the flows directly at the front face of the injector. The distance *L* is defined as the length of the annular slot in which propellants mix directly after the injector face, and *d** is the slot radial gap width.

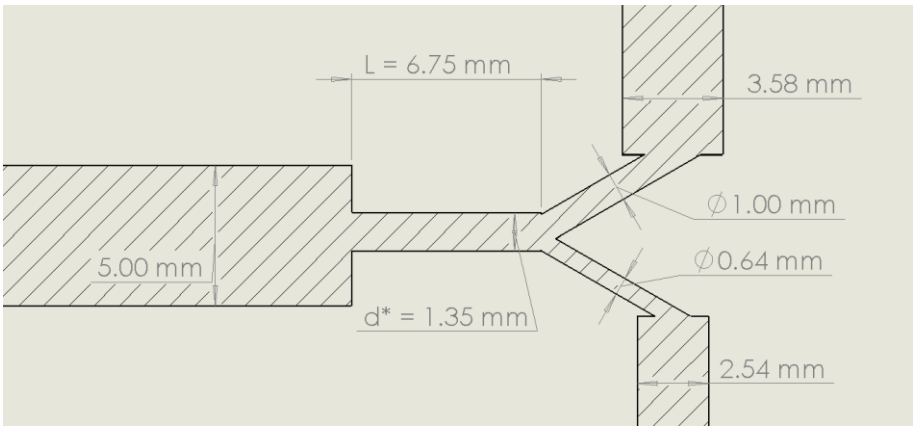

Figure 3.3 Key dimensions of flow domain (small slot, section view).

3.3 Overview of Test Cases

Simulations were conducted for single impinging injector pair with a test matrix that varied both ϕ and the injector configuration. Mass flow rate was held constant at 5 g/s total for the injector pair, or 360 g/s for the whole engine. Fuel and oxidizer inlets at the edge of the plenums were set at a pressure of 2 MPa. Only cold flow tests were considered for these simulations to examine pre-combustion mixing of the propellants. The simulation test cases listed in Table 3.2 are grouped by geometry with simulations at ϕ = 2, ϕ = 1.5, ϕ = 1, and ϕ = 0.5 for each configuration. The ratio of *L/d** is a defining feature of each slot geometry, being set at 0 (base case), 5 (small slot), and 10 (large slot). The nook injector geometry has a triangular shape with *d** increasing, and therefore the *L/d** ratio varies across it.

Table 3.2: Test Matrix

		Equivalence Ratio			
		0.50	1.0	1.5	2
Geometry	Nook	Run 2	Run 1	Run 10	Run 3
	Base (L/d* = 0)	Run 5	Run 4	Run 11	Run 6
	Small slot (L/d* = 5)	Run 7	Run 8	Run 12	Run 9
	Large slot (L/d* = 10)	Run 14	Run 13	Run 15	Run 16

Because the Run 12 configuration used the shortest slot in this study and was of the most interest, its modeling parameters were varied to examine their impact on the simulation results. The same ϕ and mass flow input conditions were used, but in Run 12b grid resolution was increased to determine its effect on the solution. In this case the base element size was halved in the mesh, resulting in an increase from 350000 elements to over 1 million. In Run 12c, the back pressure was increased to five times its current amount of 52 kPa to examine the effects of reducing injector pressure drop on mixing.

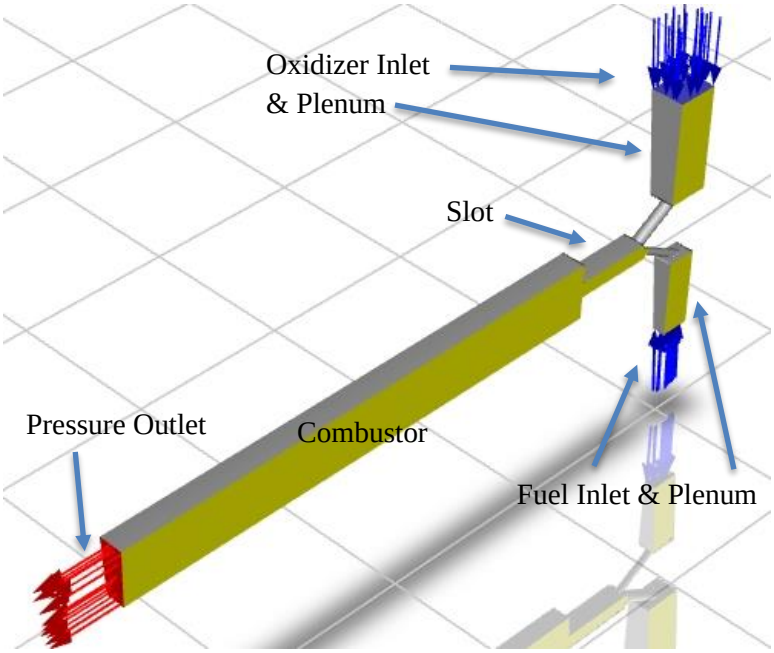

Figure 3.4: Basic setup of Run 12 (small slot, ϕ = 1)

The Reynolds number of the slot flow was computed via the expression in Eq. 2. One-dimensional adiabatic and compressible flow was assumed with complete and uniform mixing, and the slot width d^* as the length parameter. This simplifies to

$$Re = \frac{\rho_{mix} V_{slot} d^*}{\mu_{mix}} = \frac{\dot{m}_{total} d^*}{A_{slot} \mu_{mix}} \qquad [2]$$

where μ_{mix} is a mass-weighted average of the viscosities of gaseous oxygen and methane. As such, this estimate depends on the ratio of fuel and oxidizer in the mixture and comes out to 130000, 136000, 141000, and 146000 for ϕ = .5, ϕ = 1, ϕ = 1.5 and ϕ = 2 respectively.

Beyond that, in order to avoid flashback during RDRE operation, the injector channels and slot need to be small enough for the flame to be extinguished upon entering them. Turns [7] analyzed the combustion of various fuels with air and determined that a tube of up to of 2.5 mm for methane at ϕ = 1 would quench the flame. The proposed injector's fuel and oxidizer channels were much smaller than this, but further analysis is needed to predict whether the geometry would act as a flame arrester for methane and pure oxygen, especially in the slot. A rough, simplified

estimate of the heat loss for the slot is shown below in Eq. 3, which adds up the conductive heat transfer through the slot walls. The adiabatic wall temperature was assumed to be 524 K, the flame temperature was estimated at 3000 K, A is the total area of the slot surfaces and, based on the Stanton number relation for turbulent flow in a duct, h was estimated to be 7285 W/m^{2}K.

$$q_{loss} \approx h * A * \Delta T \quad [3]$$

This comes out to roughly 480W, which was then compared with the specific heat gain from combustion q_{comb}. From the mixed mass flow rate to the slot domain (0.005 kg/s) and the mass of propellant in the slot (0.946*10^{-8} kg), this heat gain is roughly 0.95 W. This implies that the slot will quench any deflagration from the combustion chamber at the conditions investigated in this study.

CHAPTER 4: Numerical Methods

The simulations in this study were performed using ANSYS FLUENT [8]. Turbulence was incorporated using the standard two equation k−ω model with shear flow corrections and production limiter options. Component mixing was enacted using a non-reacting species transport model with diffusion energy source option. Due to the complex geometry, all simulations were initialized with hybrid initialization as opposed to standard initialization. The simulations were initially converged in steady state using first order upwind spatial discretization after 2000 iterations. Then all runs were continued as pseudo transient steady state simulations, with a pseudo transient time scale factor of 1 and a flow Courant number of 0.9 to further resolve the solutions.

In order to quantify the degree to which the propellant was mixed at the desired ratio, a mixedness parameter (ξ) was computed [3]. This parameter is equal to 1 when the mass ratio of oxygen to methane is equal to that being injected, and is defined in Eq. 4 below.

$$\xi = 1 - \sqrt{\frac{\left(w_f - w_{f,opt}\right)^2}{\left(1 - w_{f,opt}\right)^2}} \qquad [4]$$

Here w_f is the oxidizer-to-fuel mass ratio from the simulation and $w_{f,opt}$ is the desired methane-to-oxygen ratio for a given experiment. This was implemented in ANSYS using a custom field function, which calculated this value for each element in the steady state simulation. Contour plots of mixedness and CH_4 mass fraction formed the bulk of the data used to assess the impact of slot geometry on propellant mixing.

4.1 Meshing

To reduce computational cost the fluid domain was split radially into 1/72 of its original size (corresponding to one fuel-injector pair) for the 50 mm annular configurations. Both plenums were modeled as part of the simulation domain. Inlet mass flow boundary conditions were specified at the inlets of the plenums with the mass fraction of methane and oxygen set to unity. The outlet of the domain was a pressure outlet boundary condition with pure nitrogen reverse flow to account for possible back flow from the dump tank that was distinct from the fuel and oxidizer gases. No-slip wall boundary conditions were used for all the solid walls of the domain, while the sides of the domain were modeled as slip walls, since they are symmetry planes.

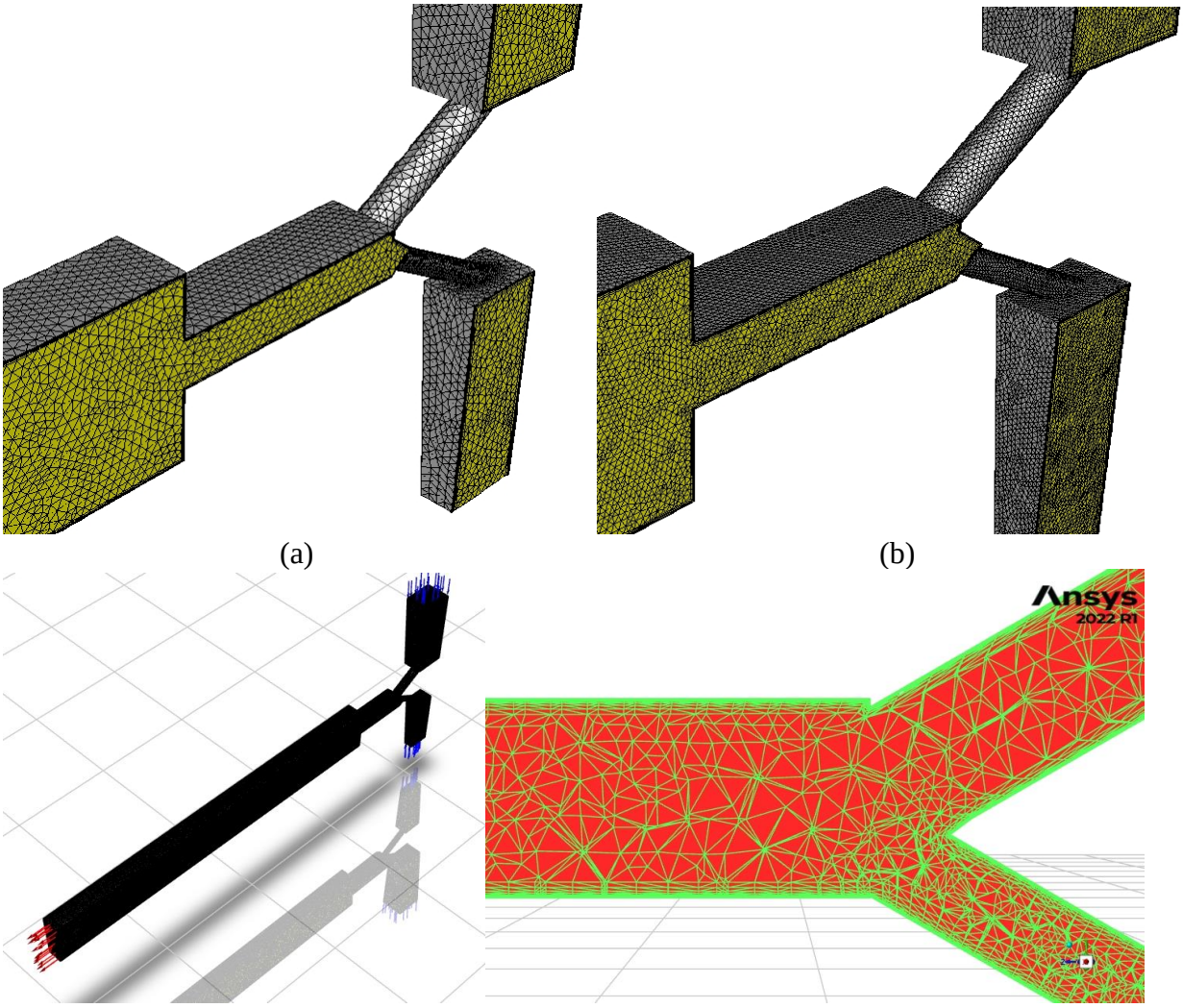

Figure 4.1: Render of (a) coarse mesh for Run 12 (b) fine mesh for Run 12b (c) full view of mesh (d) magnified view of slot in coarse mesh

The mesh for this study was an unstructured tetrahedral mesh with wedge elements forming the inflation layer at the walls to capture the boundary layer flow. Boundary layer inflation was specified to be 10 layers with a growth rate of 1.4. A mesh convergence study consisting of two cases was performed using the mesh for the small slot ($L/d^* = 5$) configuration as a baseline, while injecting the propellant components at flow rates corresponding to $\phi = 1.5$. The baseline and most refined meshes are shown in Fig. 4.1 for comparison. To monitor convergence of the species mixing aspect of the flow field, planar averages of mixedness at various locations were compared across all simulations, as well as Mach number, velocity, and total pressure at the end of the slot.

CHAPTER 5: Computational Results and Discussion

The locations of the planes were defined qualitatively to compare the results across different geometries. All planes were oriented normal to the axial direction of the annulus (z-axis). Along this axis were the locations referred to as - the flow impingement point, the midway point of the slot, the end of the slot, the 5 mm and 10 mm fill heights after the slot exit, the midway point of the combustion chamber, and the end of the combustion chamber. The fill height is the axial length (measured from the injector face) to which the mixed propellant is able to travel within the annulus before the detonation wave hits it. Estimates of this distance for a wide range of propellant injection conditions range from 3 mm to 10 mm, which guided the choice of fill heights chosen here for reference [9,10]. Since separation distances between these planes listed in Table 3.3 vary based on the injector configuration. The axial direction of the chamber was parallel to the z-axis in the setup, so the origin z = 0 was taken to be the impingement point to maintain consistency of the injector parameters. The distances for the mid-channel and end of channel are provided relative to the plane at the exit of the slot.

Table 3.3: Plane Locations for Mixedness Measurement

	Axial Z-Position (mm)						
	Impingement Point	Mid-Slot	End of Slot	5mm Fill Height	10mm Fill Height	Mid-Channel	End of Channel
Nook	0	0.6	1.2	6.2	11.2	25.0	40.0
Base (L/d* = 0)	0	N/A	N/A	5.0	10.0	25.0	40.0
Small slot (L/d* = 5)	0	3.5	6.7	11.7	16.7	25.0	40.0
Large slot (L/d* = 10)	0	6.7	13.3	18.3	23.3	25.0	40.0

Several of the aforementioned planes are shown in Fig. 5.1, where they construct a skeletal view showing several cross sections of the flow domain, including the azimuthal midplane. In addition, a side view of the entire domain illustration is shown in Appendix B with the plane locations labeled in the case of the small slot ($L/d^* = 5$).

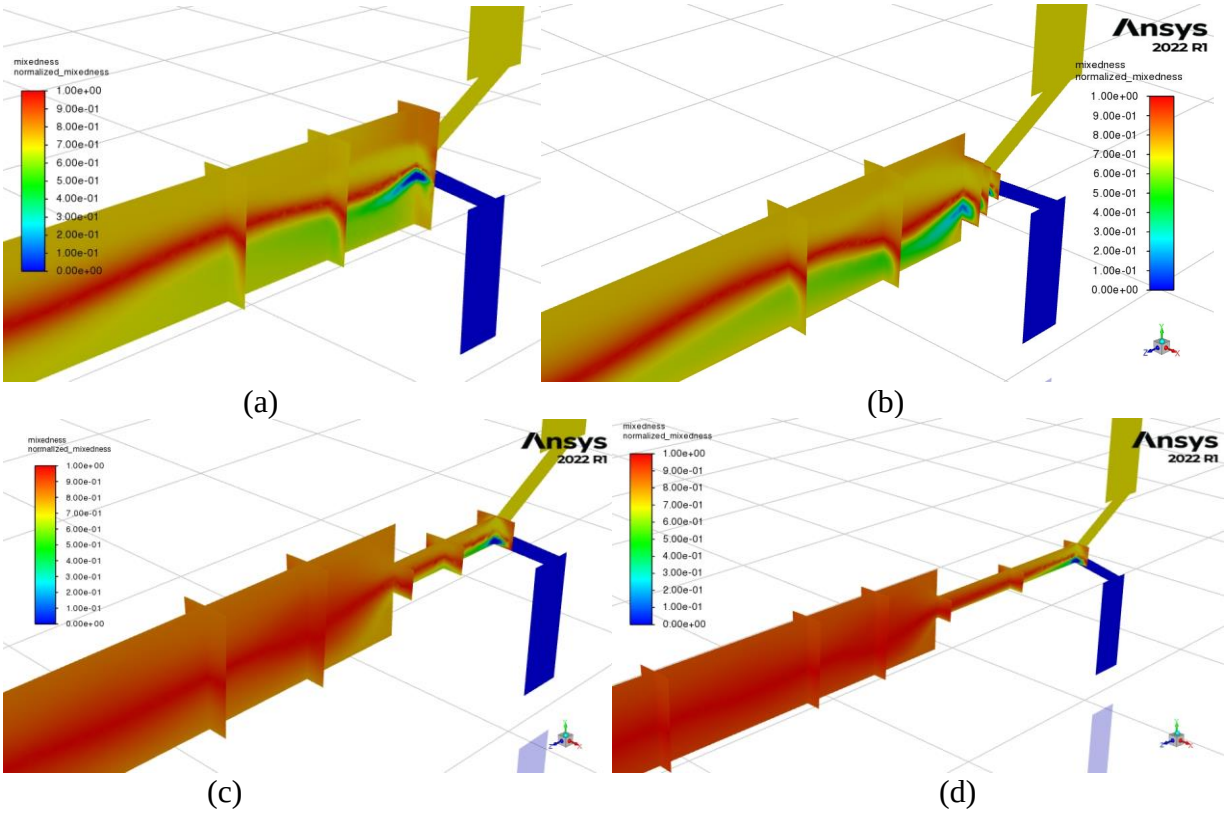

Figure 5.1: Mixedness midplane + cross-sectional plot for ϕ = 1 in (a) base case (b) nook injector (c) small slot (d) large slot

Across all 16 main simulations, the impact of geometry and ϕ are clear and consistent. All three new geometries show increased mixedness at every location downstream from the injector face as opposed to the base case. The planar averages of mixedness at these locations listed in Table 5.1 prove this quantitatively, and they are plotted in Fig. 5.2 and in Appendix B.

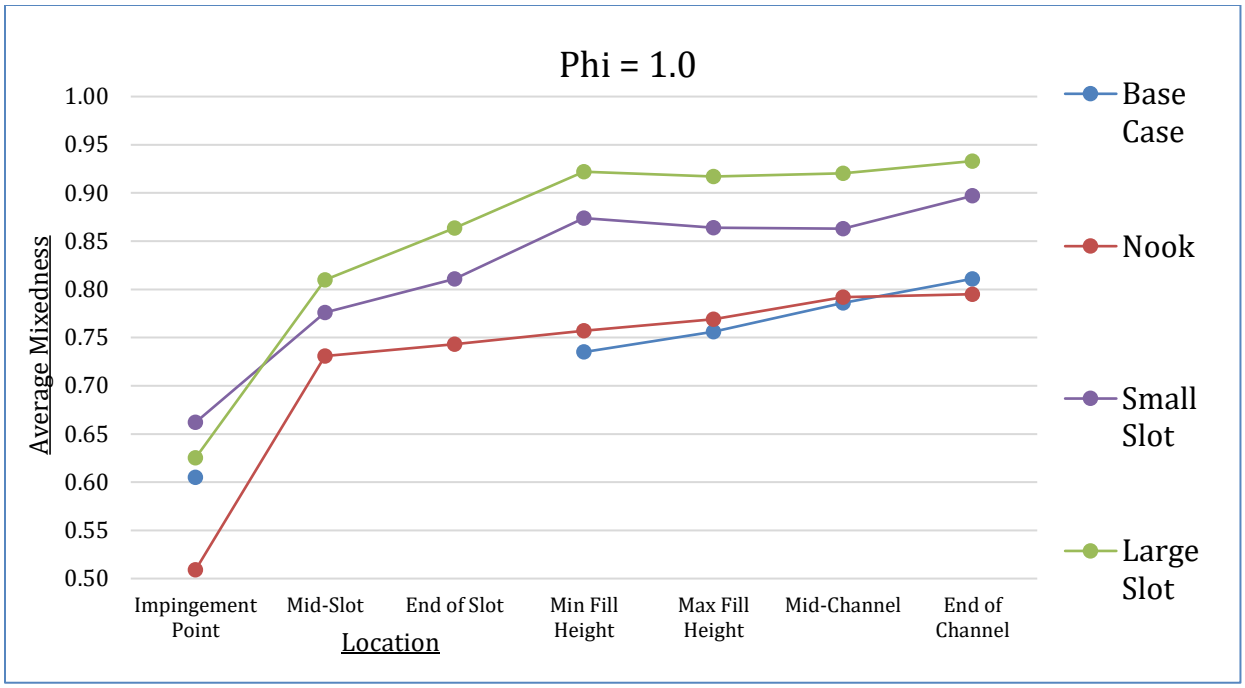

Figure 5.2: Planar mixedness averages across geometries for ϕ=1

From this, a positive correlation between mixedness and slot *L/d** ratio can be reasonably assumed. Across all four values of ϕ, the longer slot achieved the highest mixedness averages at every location downstream of the injector face. As for the effect of ϕ on the mixedness, two main results were observed. First, ϕ=1.0 and ϕ=1.5 typically resulted in slightly higher mixedness at most locations (see Fig. B.20). Second, ϕ determined the momentum imbalance in the radial direction which resulted in one of the two jets dominating the flow and pushing the region of highest mixedness radially outward for higher ϕ and inward for lower ϕ. This region was centered closest to the middle (22.5 mm radial distance) of the annulus for ϕ = 1. It should be noted that momentum balance occurs around ϕ = 3 for this area ratio at these injection angles, so this observation is likely due to the three-dimensional geometry preventing full momentum transfer from the oxidizer stream.

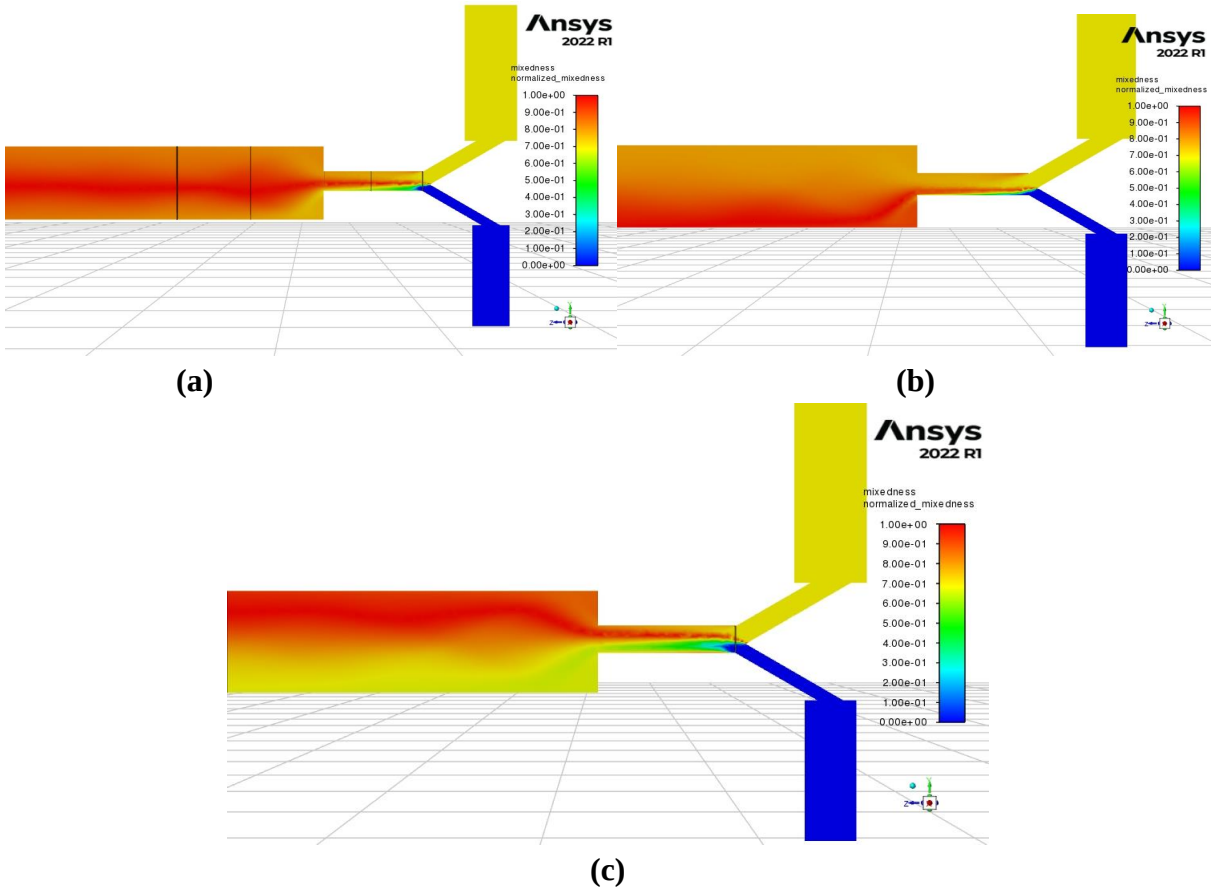

Figure 5.3: Mixedness mid-plane plot for small slot in (a) ϕ = 1 (b) ϕ = 0.5 (c) ϕ = 2

5.1 Validation of Simulation Results

The solutions given by the simulations were validated in multiple ways to ensure that the result was consistent and robust. A great deal of time was spent ensuring that the converged solution was accurate and matched up with observations made experimentally and in previous simulations of mixing flow in 1-inch and 10 mm diameter engines. One way to verify this is by looking at the Mach number of the fuel and oxidizer flows as they go from the plenums to the channels and ultimately the annulus, as pictured in Fig. 5.4.

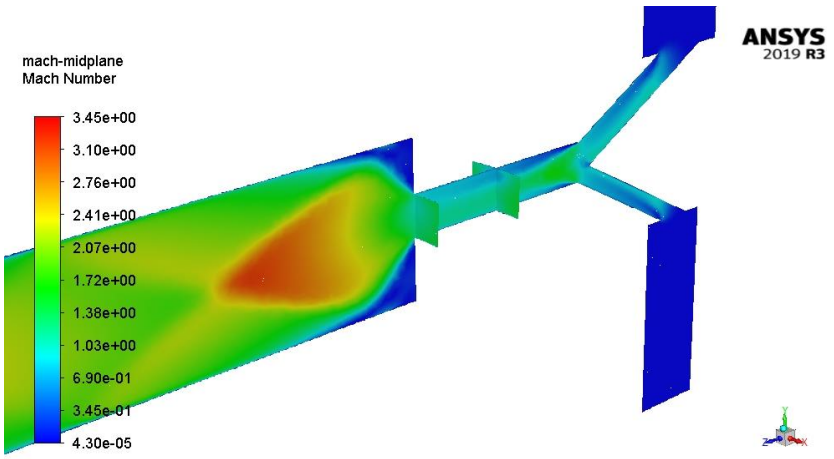

Figure 5.4: Midplane Mach contour plot of Run 12 (with cross sections in slot)

Due to the pressure ratio between the plenums and the injector channels, the fuel and oxidizer lines were choked, and reached roughly uniform Mach 1 just before impingement[3]. In the oxidizer line, this was observed in all 16 trials for the 50mm engine. However, lower equivalence ratio Runs consistently showed that the momentum domination of the oxidizer line caused the fuel to not choke fully at the exit of its injector port. This was deemed to not be a pressing issue since it still mixes with the oxidizer line and supersonically expands into the combustion chamber as expected.

Next, a mesh refinement case was performed on Run 12, with mesh resolution increased by 234%. Mixedness averages remained identical within two decimal places, as shown in Table 5.2, and the contour plots looked the same (see Figure B.12.2)

Table 5.2: Variations on Run 12

					Average Mixedness						
Run (#)	# of Mesh Elements	Back Pres (kPa)	Mach at end of slot	Vel at end of slot (m/s)	Impinge Point	Mid-Slot	End of Slot	5 mm Fill Height	10 mm Fill Height	Mid-Comb	End of Comb
12	366842	53	1.122	355	0.652	0.782	0.810	0.856	0.857	0.865	0.884
12B	1171354	53	1.174	370	0.688	0.779	0.806	0.849	0.844	0.855	0.873
12C	366842	265	1.108	351	0.652	0.782	0.810	0.844	0.856	0.877	0.912

An additional simulation (Run 12c) was conducted with all parameters held the same from Run 12, but with the back pressure set to 265125 Pa (163800 Pa gauge) instead of 53025 Pa (-48300 Pa gauge). The overall result was larger recirculation zones, as well as significant confinement and damping of the flow as pictured below in Fig. 5.5, but mixedness actually increased downstream of the injector.

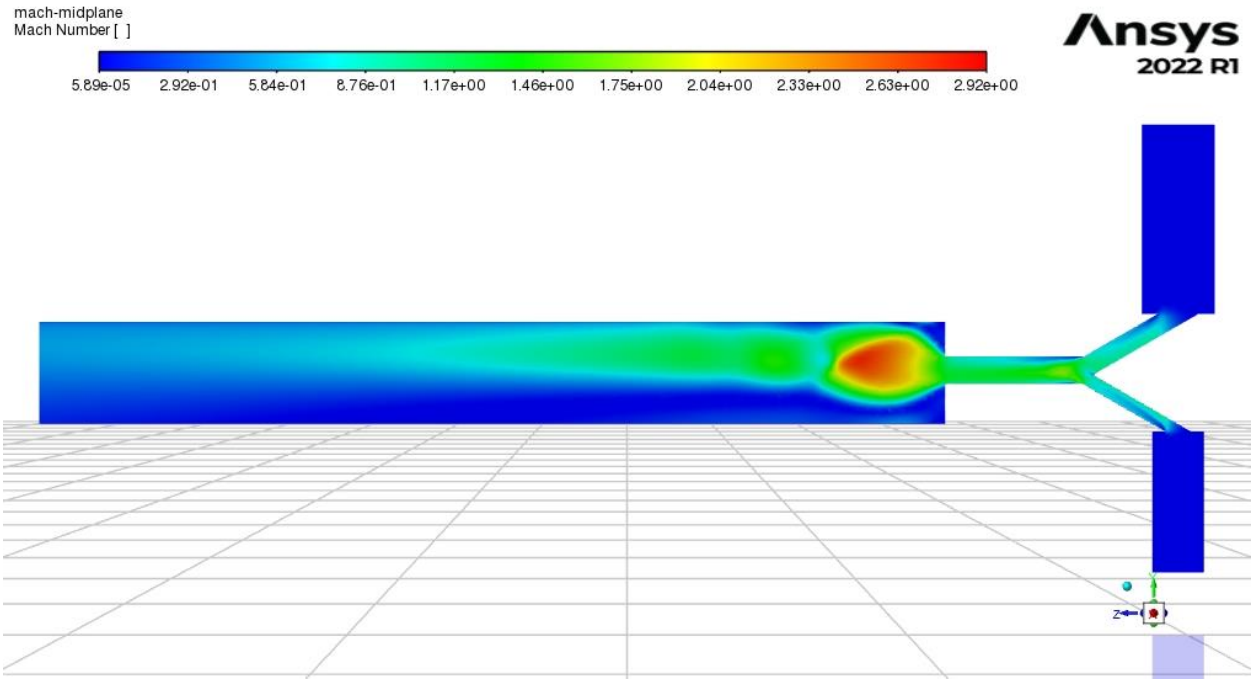

Figure 5.5: Mach number midplane plot of Run 12c

(a)

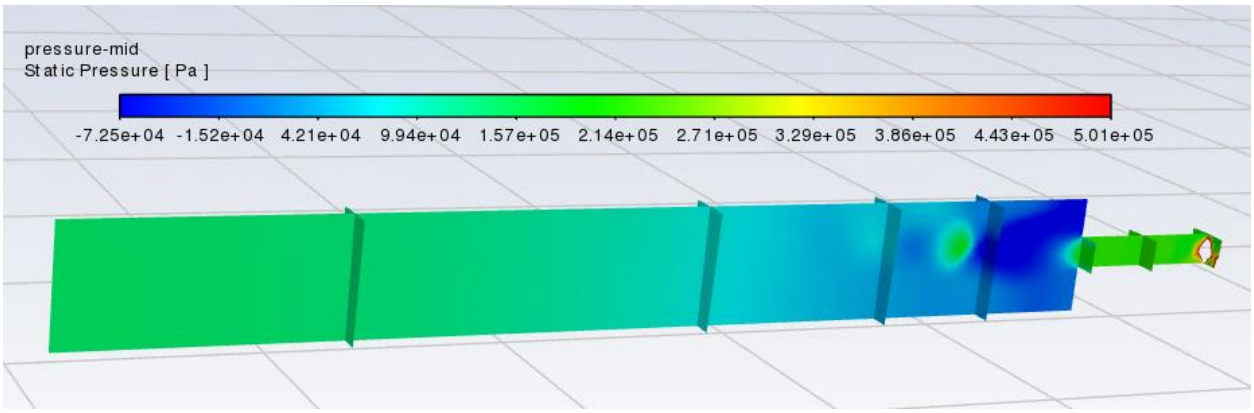

Figure 5.6: Pressure plot of Run 12c (a) center plane (b) adjusted range with cross-sections

The pressure readings appear much more anomalous here in comparison with Runs 12 and 12b. Due to the presence of large recirculation zones in the axial direction, the pressure averages are higher downstream of the slot face. A Mach diamond appears to form, but the supersonic jet dissipates and slows down, with Fig. 5.5 indicating that the flow at the end of the combustor is subsonic. This is still a preliminary result, and future simulations must further investigate the effect of added back pressure.

Table 5.3: Static pressure across variations on Run 12

			Average Static Pressure (kPa gauge)						
Run #	# of Elements in Mesh	Back Pressure (kPa)	Impinge Point	Mid-Slot	End of Slot	5 mm Fill Height	10 mm Fill Height	Mid-Comb	End of Comb
12	366842	53	356	219	185	-53	-54	-55	-51
12B	1171354	53	342	228	192	-37	-61	-55	-49
12C	366842	265	373	232	201	23	74	107	154

CHAPTER 6: Conclusion

Overall, the results of this study indicated that subsurface impingement mixes propellants faster than above-surface impingement. Adding a thin channel slot extension further improved mixing, which was quantified by a planar average of mixedness, ξ, with longer channels having even more improvement. This feature also reduced the azimuthal mixture differences in the flow prior to its injection into the combustor. Compared with previous computational results on 10 mm

and 25.4 mm diameter engine configurations with above-surface impingement [3], contour plots of these geometries consistently showed the region where ξ was nearly 1 to be much larger and more evenly spread across the combustion annulus. Since better mixed propellants offer potential for reducing pre-detonation burning, the implementation of this method for RDRE injectors can increase their performance.

Future Work

The development of this new method can progress in several different directions. To begin with, the maximum flowrates must be determined that will not choke the slot exits nor have detonation cell sizes small enough to propagate given the current cell width. Beyond that, the slot width d* must be varied in future simulations and experiments, as smaller slots can operate at higher combustor mass fluxes without pre-detonating in the slot up to the point where the slot exit is choked. Therefore, implementation of a diverging slot may increase the range of operating mass fluxes without choking the slot exit. For space propulsion applications, however, the exit of the slot must stay choked, so the minimum slot width for supersonic outflow at nominal mass flux will need to be determined. Lastly, future investigations can implement fluidic diode slot configurations with high diodicity to enable larger flow rates for a given slot width. These can reduce backflow of propellants, which occurs due to the high pressures generated by the detonative combustion process in the annulus.

Once the steady-state species transport for all these configurations are investigated, the most optimized injector design can proceed on to the next stage – reactive flow simulations and ultimately fabrication and hot-fire testing, where detonation engine performance can be fully assessed.

Bibliography

[1] Koch, J. V., “Nonlinear Dynamics of Rotating Detonation Waves,” Ph.D. thesis, William E. Boeing Department of Aeronautics and Astronautics, University of Washington, Seattle, WA, 2020. URL http://hdl.handle.net/1773/45431.

[2] Gamba, M., Feleo, A., Shepard, J., Chacon, F., “State-to-State Model for Rotating Detonation Combustors”, 28th ICDERS, June 19-24, 2022

[3] Roberts, Quentin, “Investigation of Pre-Ignition Propellant Mixing in Rotating Detonation Rocket Engine ,” M.S. thesis, William E. Boeing Department of Aeronautics and Astronautics, University of Washington, Seattle, WA, 2023.

[4] Washington, Malik R, “Radial Injector Mixing Effects on Detonation Zone Position in Rotating Detonation Engine,” M.S. thesis, William E. Boeing Department of Aeronautics and Astronautics, University of Washington, Seattle, WA, 2019.

[5] Mendez, Daniel, “Turbulent Methane Oxygen CFD Thermal Effects on Rotating Detonation Engine,” M.S. thesis, William E. Boeing Department of Aeronautics and Astronautics, University of Washington, Seattle, WA, 2019

[6] Burke, R., Rezzag,T., Kotler, A., and Ahmad, K., “The Effect of Fuel Partial Premixing on Rotating Detonation Waves”, 28th ICDERS, June 19-24, 2022

[7] Turns, S. R. (2000). *An Introduction to Combustion*. McGraw-Hill Science, Engineering & Mathematics.

[8] ANSYS, Inc., ANSYS® Fluent Revision 19.5.0, Southpointe 2600 ANSYS Drive, Canonsburg, PA, 2019.

[9] Mundt, T., “Geometric Scaling of Cylindrical Rotating Detonation Rocket Engine Combustors,” PhD Thesis, William E. Boeing Department of Aeronautics and Astronautics, University of Washington, Seattle, WA, 2023. http://hdl.handle.net/1773/50198

[10] Knowlen, C., Mundt, T., and Kurosaka, M., “Experimental Results for 25-mm and 51- mm Rotating Detonation Rocket Engine Combustors,” *Shock Waves,* Vol 33, 237–252 (2023). https://doi.org/10.1007/s00193-023-01120-x.

APPENDIX A:

Additional Fuel Mass Fraction Contours

The following plots show the mass fraction of CH4 through the simulation domain. Stoichiometric mixing corresponds to a value of 0.25, which is represented on the legend as neon blue. Some plots include the cross-sectional planes (normal to the axial direction) across which measured values were averaged. This serves to establish that radial symmetry in the mixing was observed. Runs were numbered chronologically, but the key parameters being varied are listed in each figure. For each geometry, the influence of ϕ on the shape of the fully mixed region can be observed.

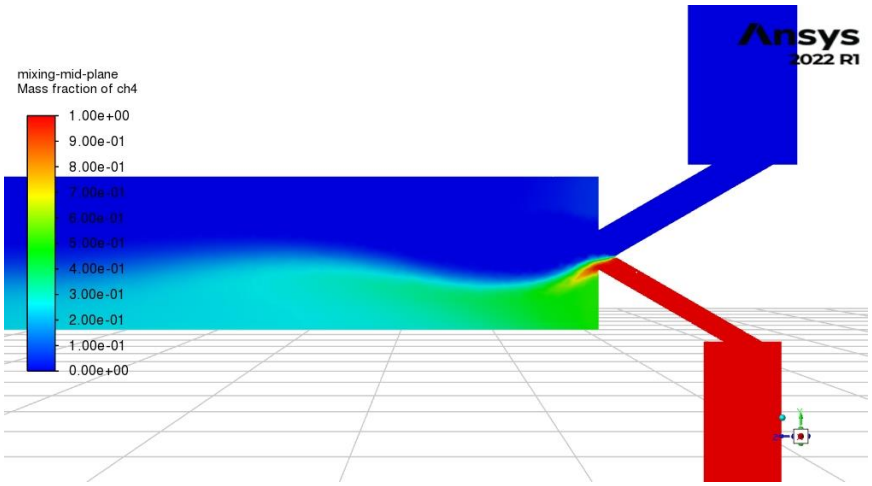

Figure A.1: Injector center plane contours of w_f for Run 5(Base Case, ϕ = .5).

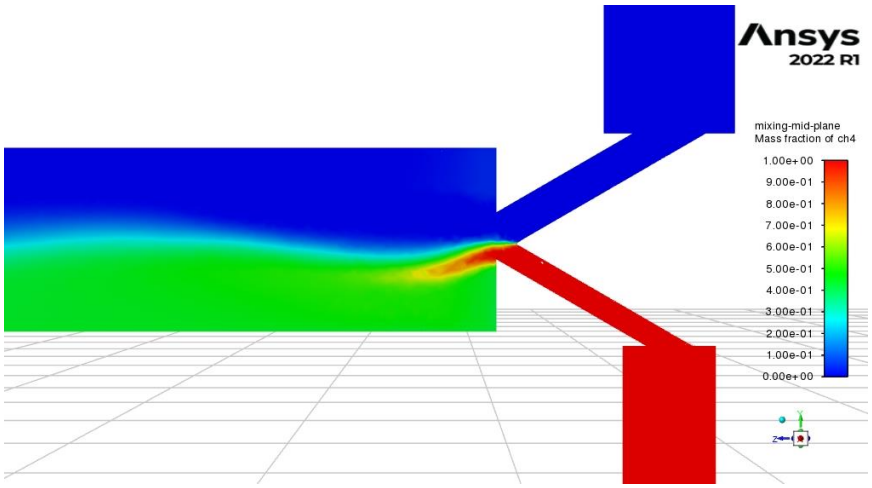

Figure A.2: Injector center plane contours of w_f for Run 4(Base Case, ϕ = 1).

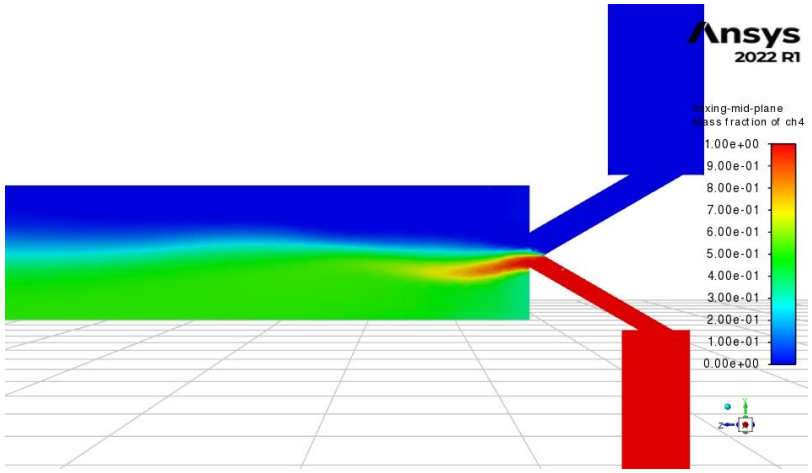

Figure A.3: Injector center plane contours of w_f for Run 11 (Base Case, ϕ = 1.5).

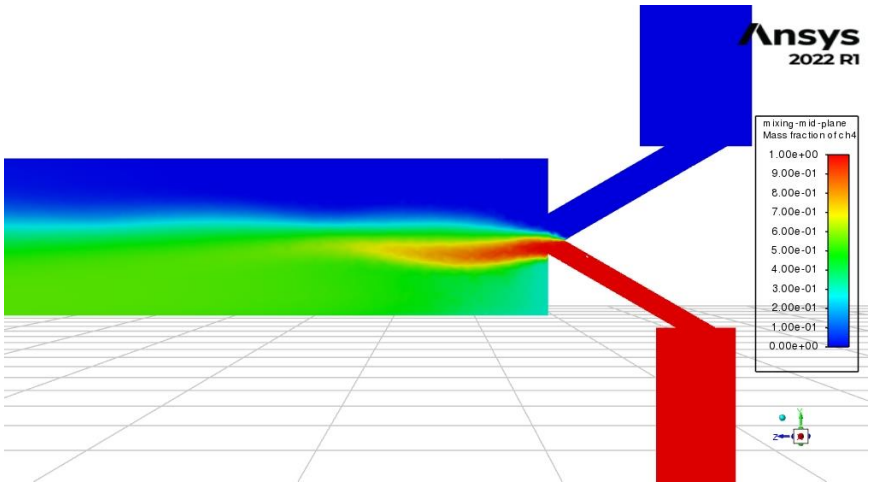

Figure A.4: Injector center plane contours of w_f for Run 6(Base Case, ϕ = 2).

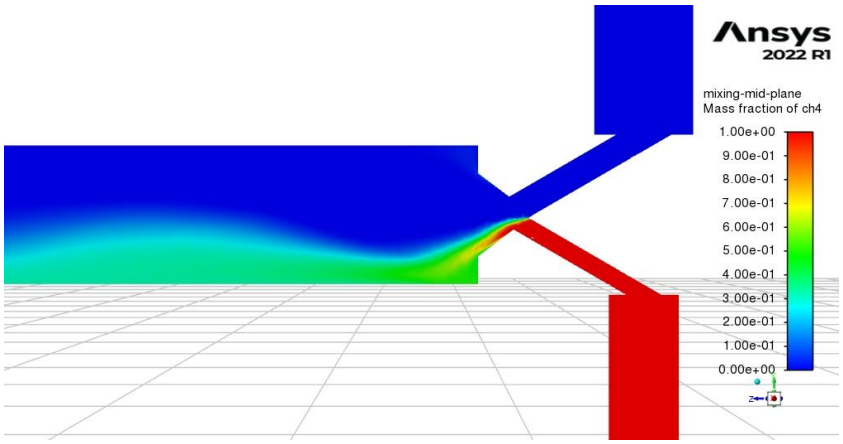

Figure A.5: Injector center plane contours of w_f for Run 2(Nook, ϕ = .5).

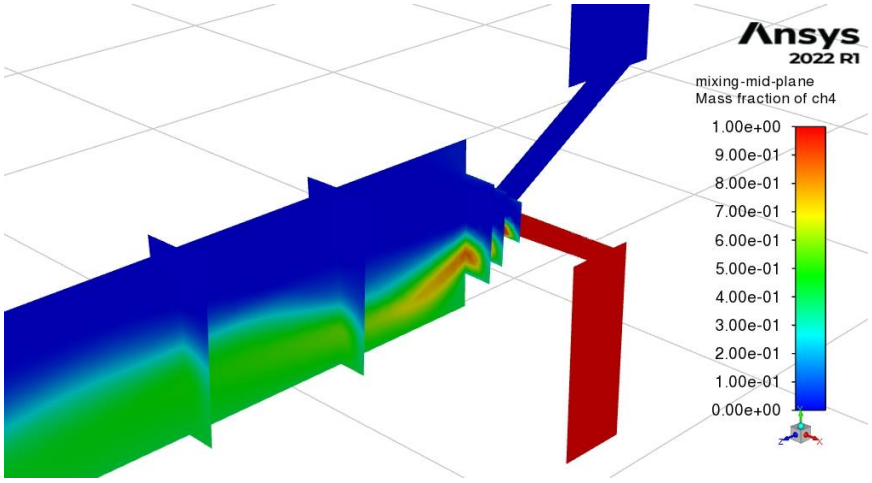

Figure A.6: Injector center plane + cross section contours of w_f for Run 1(Nook, ϕ = 1).

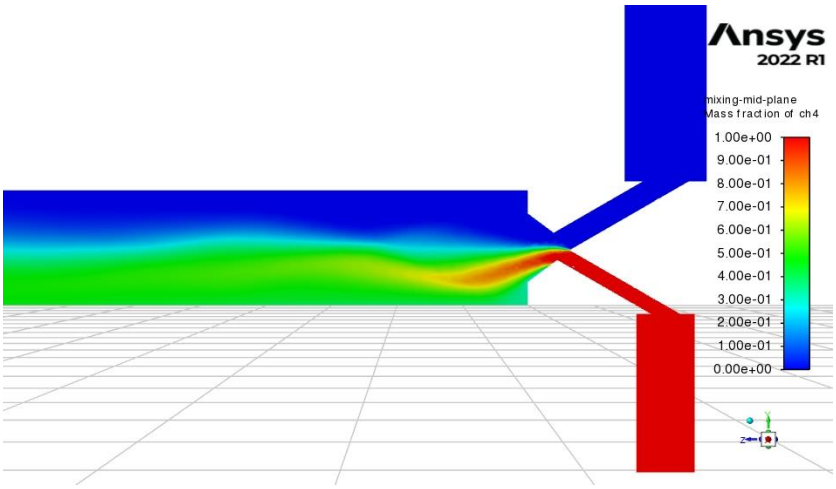

Figure A.7: Injector center plane contours of w_f for Run (Nook, ϕ = 1.5).

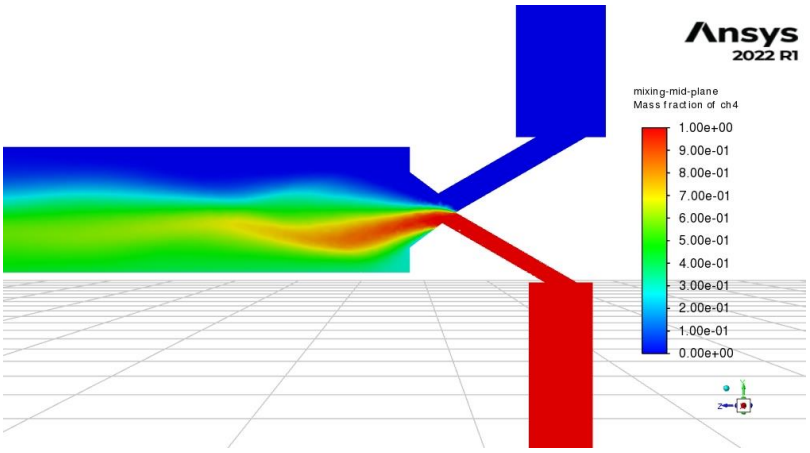

Figure A.8: Injector center plane contours of w_f for Run 3(Nook, ϕ = 2).

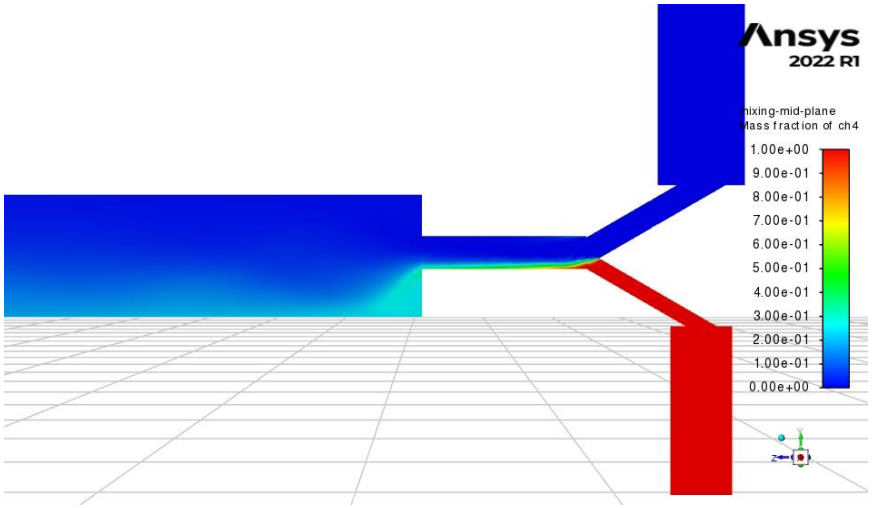

Figure A.9: Injector center plane contours of w_f for Run 8(Small Slot, ϕ = .5).

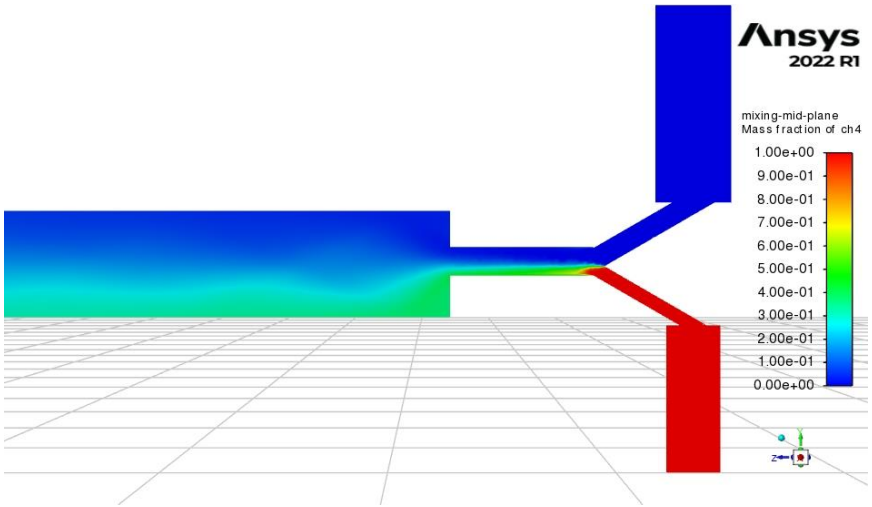

Figure A.10: Injector center plane contours of w_f for Run 7(Small Slot, ϕ = 1).

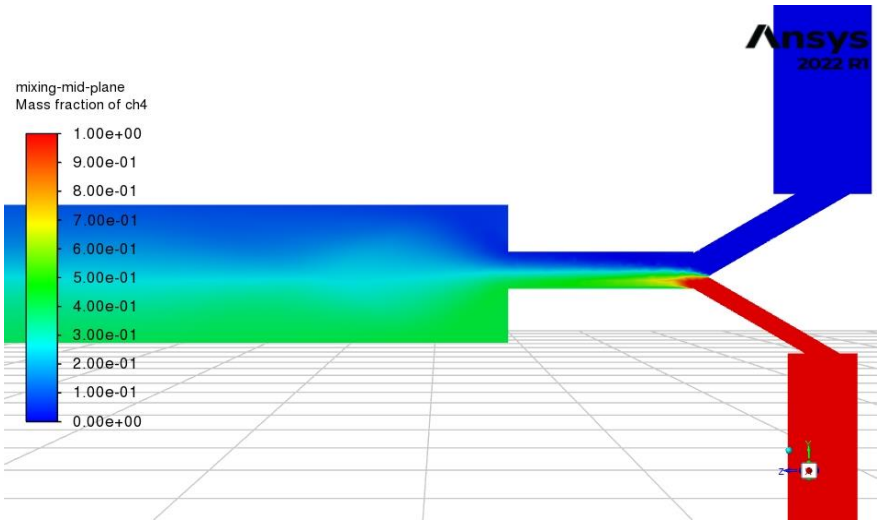

Figure A.11: Injector center plane contours of w_f for Run 12 (Small Slot, ϕ = 1.5).

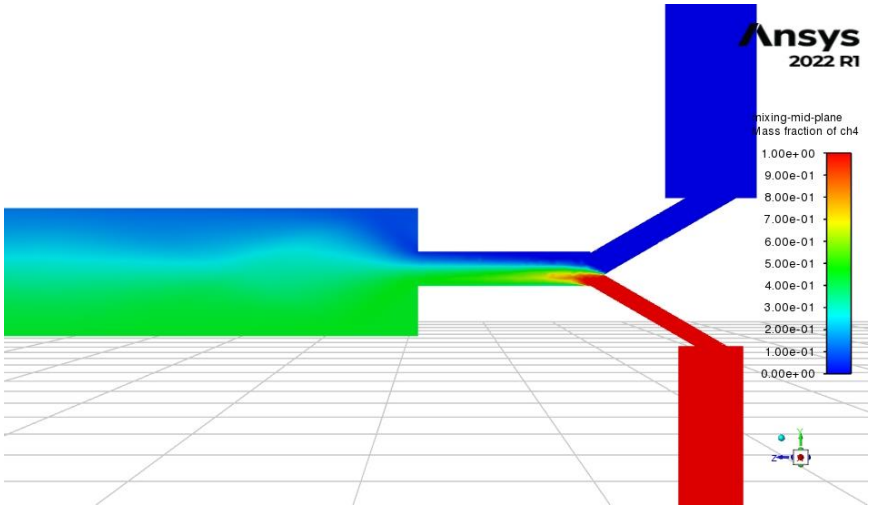

Figure A.12: Injector center plane contours of w_f for Run 9(Small Slot, ϕ = 2).

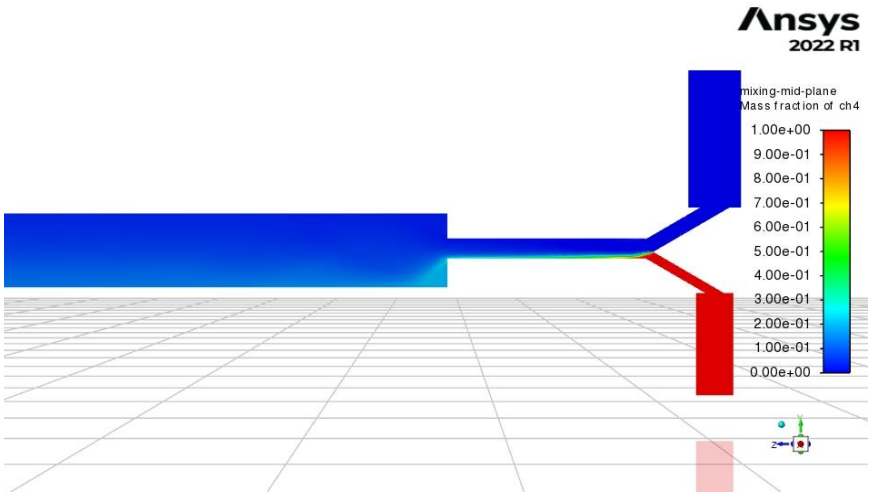

Figure A.13: Injector center plane contours of w_f for Run 14(Large Slot, ϕ = .5).

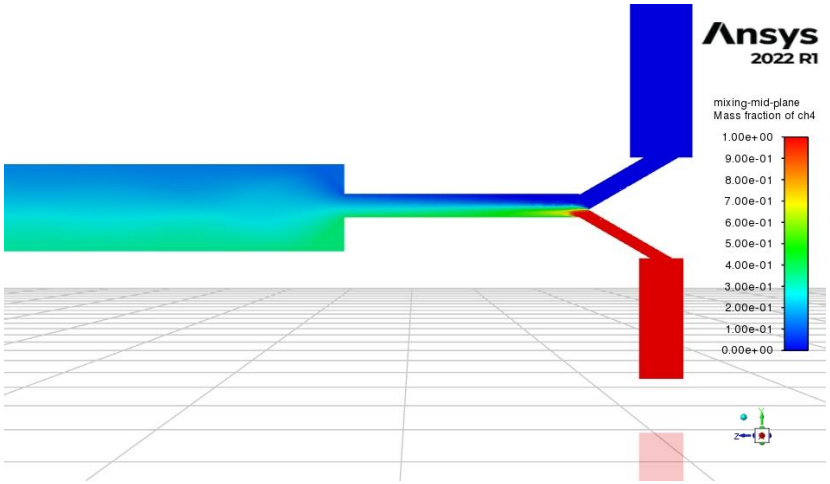

Figure A.14: Injector center plane contours of w_f for Run 15(Large Slot, ϕ = 1.5).

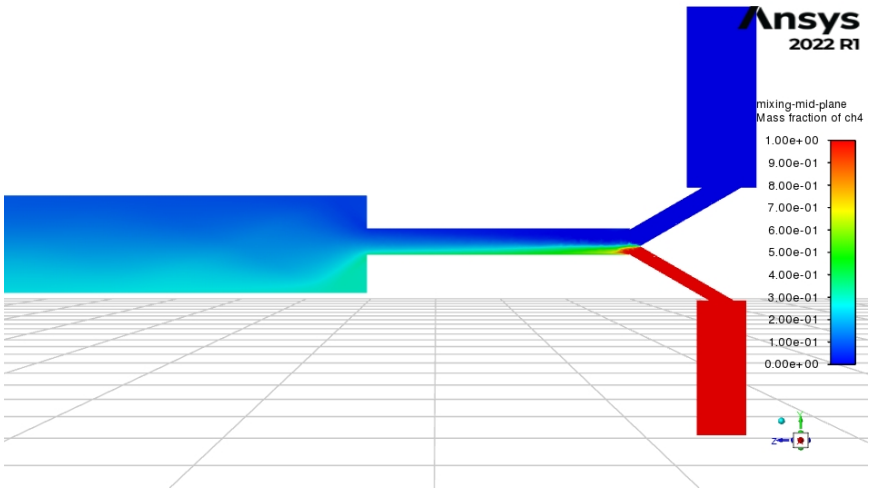

Figure A.15: Injector center plane contours of w_f for Run 13(Large Slot, ϕ = 1).

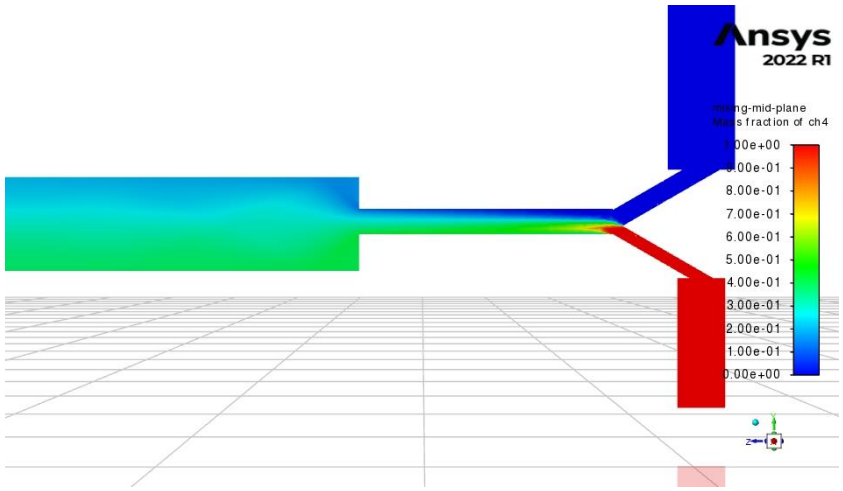

Figure A.16: Injector center plane contours of w_f for Run 16(Large Slot, ϕ = 2).

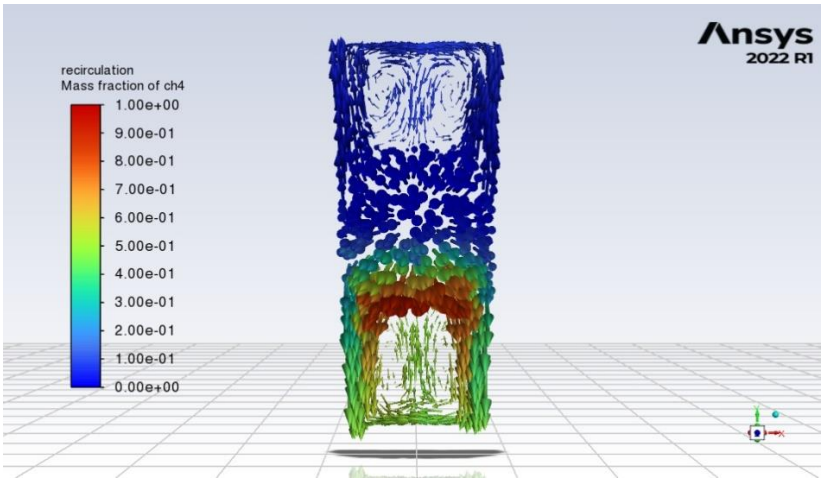

Figure A.17: Flow field normal to axial direction, minimum fill height (Run 4), vectors colored by CH4 mass fraction - observe recirculation in azimuthal direction

APPENDIX B:

Additional Mixedness Contours

The following plots show the mass fraction of the mixedness parameter ξ through the simulation domain. Stoichiometric mixing corresponds to a value of 1.00, which is represented on the legend as red. These plots further highlight the influence of ϕ on the shape of the fully mixed region, showing not only which stream dominated the momentum, but also dispersion of the mixed region throughout the combustor.

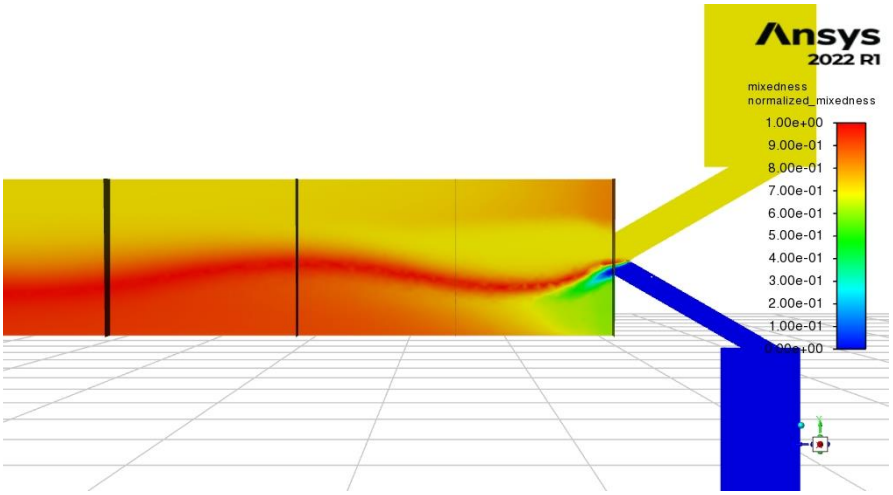

Figure B.1: Injector center plane contours of ξ for Run 5(Base Case, ϕ = .5).

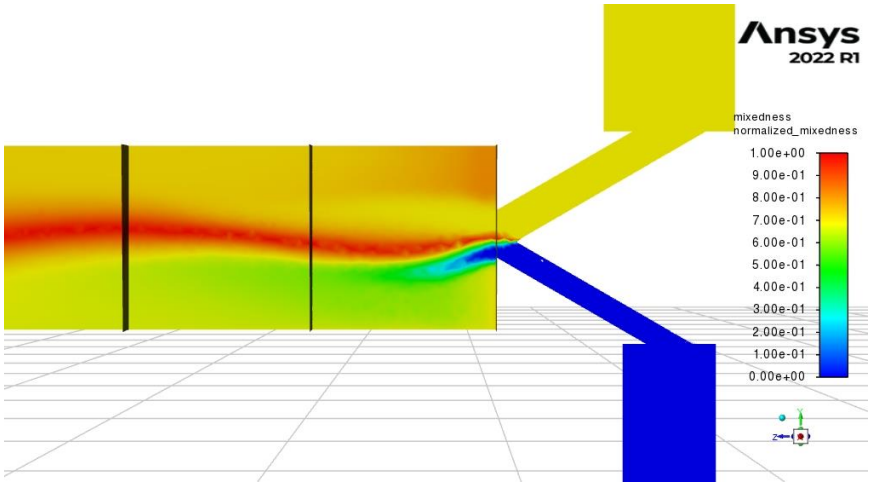

Figure B.2: Injector center plane contours of ξ for Run 4(Base Case, ϕ = 1).

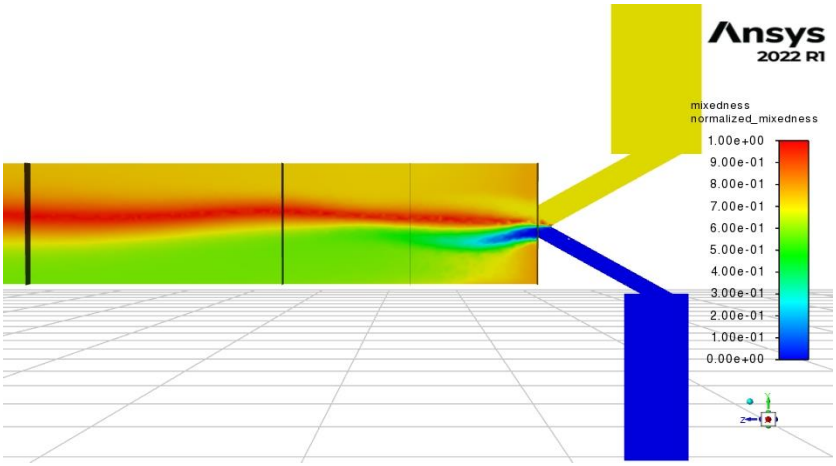

Figure B.3: Injector center plane contours of ξ for Run 1(Base Case, ϕ = 1.5).

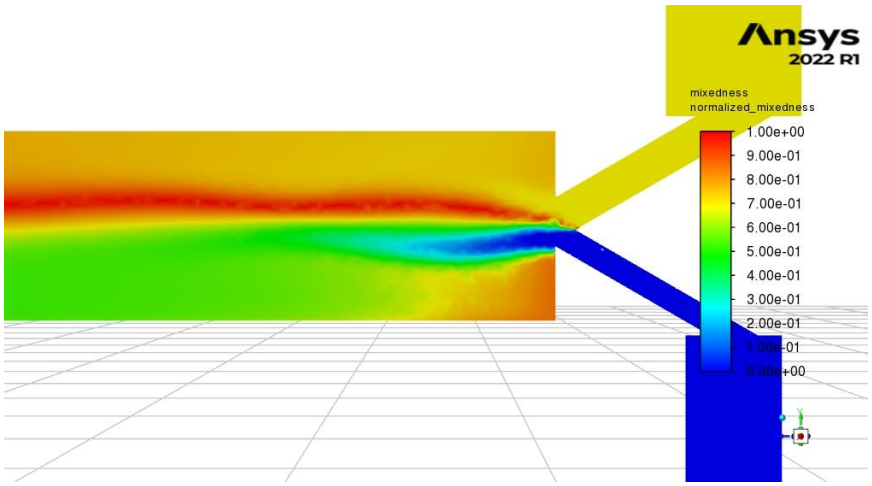

Figure B.4: Injector center plane contours of ξ for Run 6(Base Case, ϕ = 2).

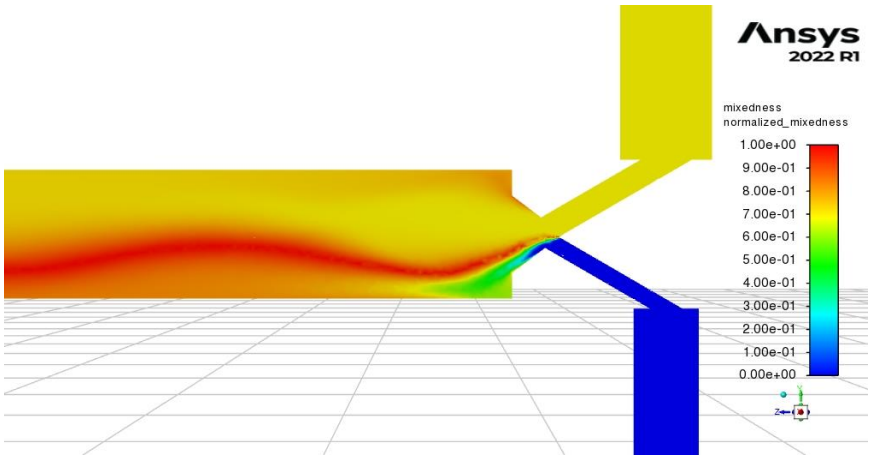

Figure B.5: Injector center plane contours of ξ for Run 2(Nook Injector, ϕ = .5).

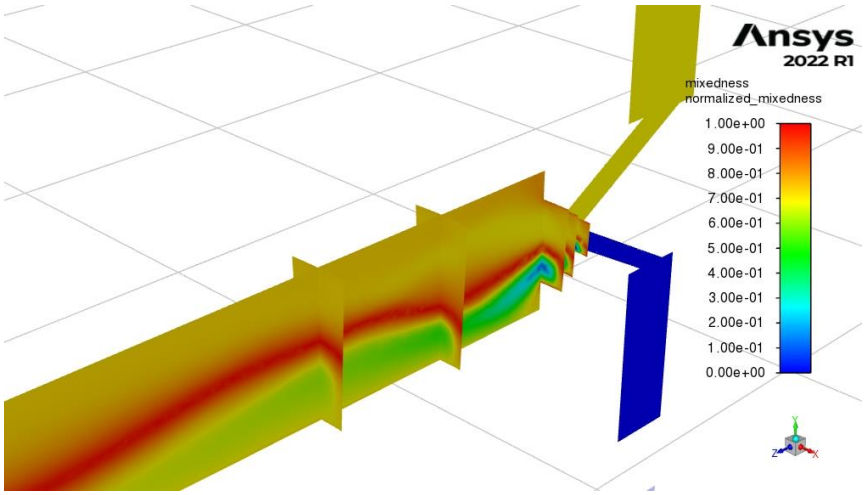

Figure B.6: Injector center plane + cross section contours of ξ for Run 1(Nook Injector, ϕ = 1).

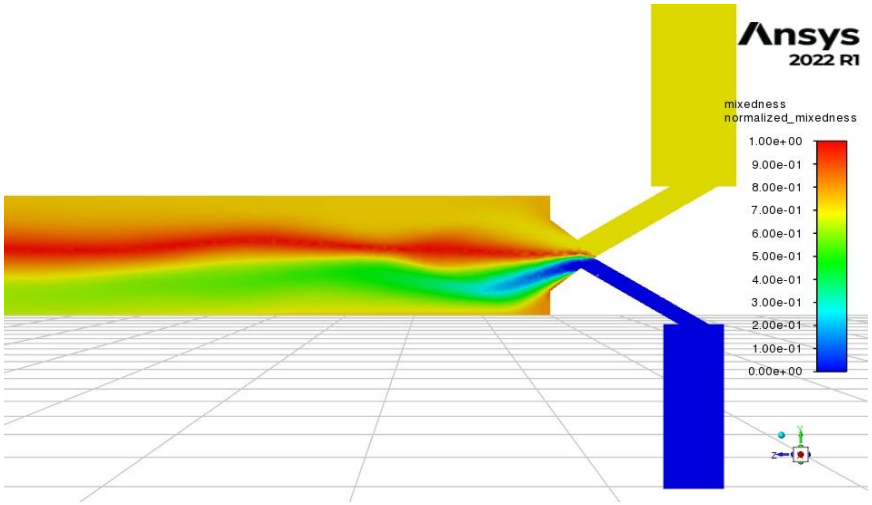

Figure B.7: Injector center plane contours of ξ for Run 10(Nook Injector, ϕ = 1.5).

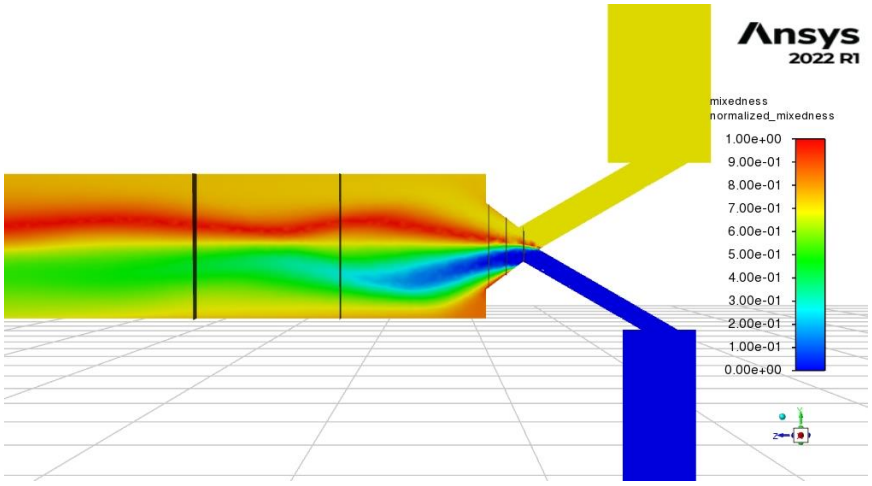

Figure B.8: Injector center plane contours of ξ for Run 3(Nook Injector, ϕ = 2).

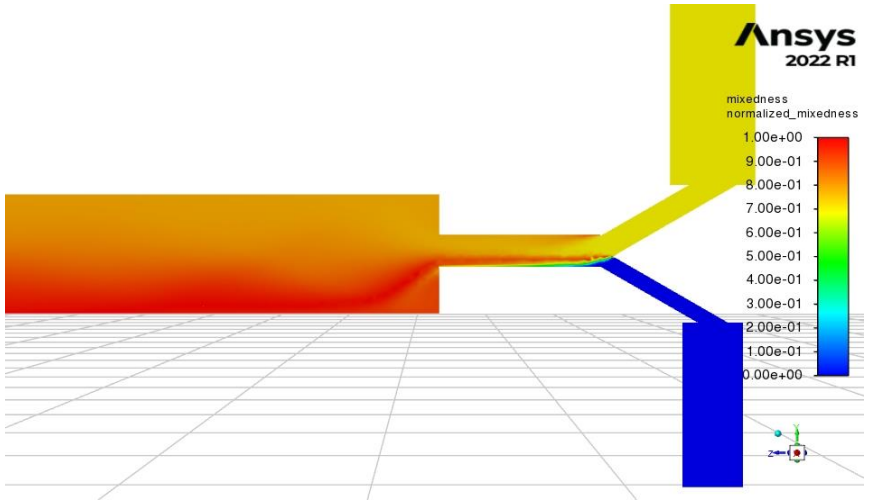

Figure B.9: Injector center plane contours of ξ for Run 8(Small Slot, ϕ = .5).

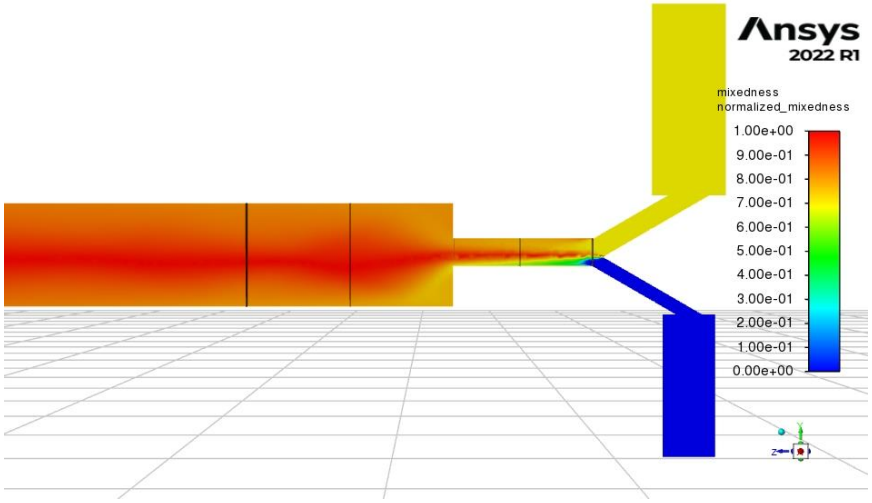

Figure B.10: Injector center plane contours of ξ for Run 7(Small Slot, ϕ = 1).

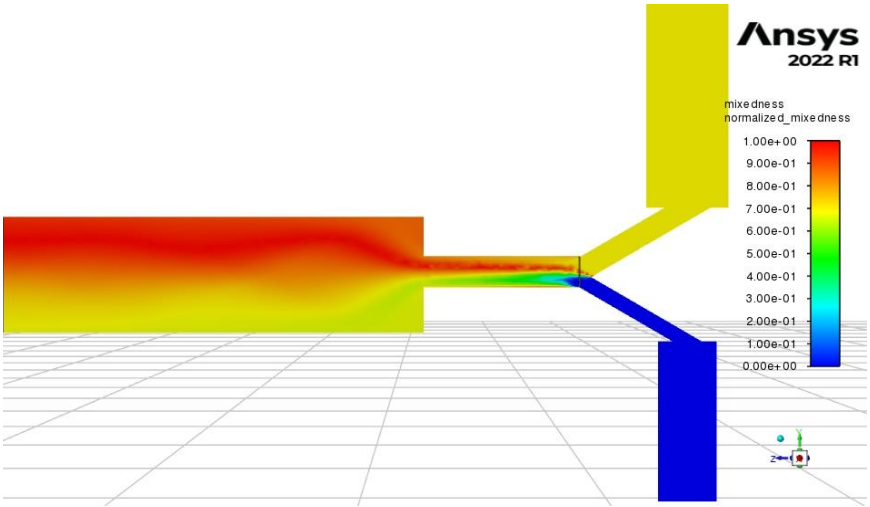

Figure B.11: Injector center plane contours of ξ for Run 9(Large Slot, ϕ = 2).

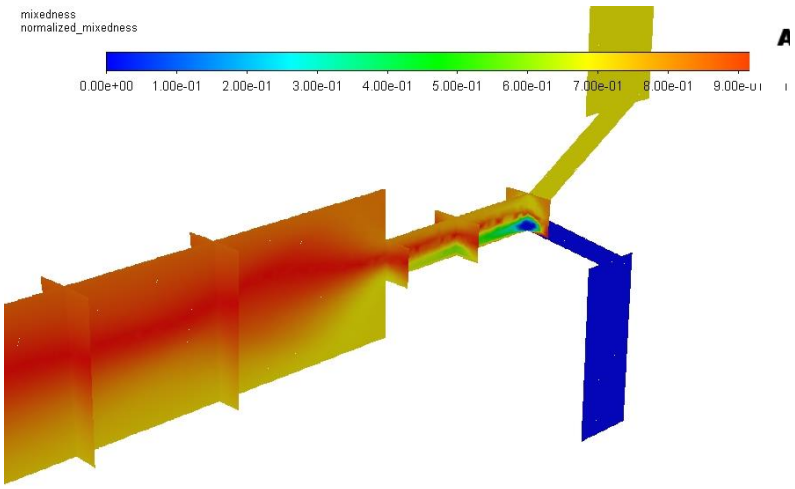

Figure B.12.1: Injector center plane + cross section contours of ξ for Run 12(Small Slot, ϕ = 1.5).

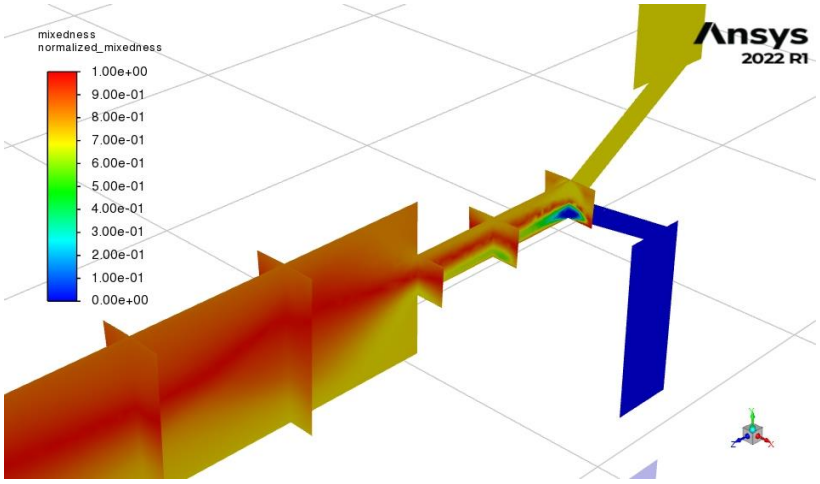

Figure B.12.2: Injector center plane + cross section contours of ξ for Run 12b (Small Slot, ϕ = 1.5 with higher resolution mesh).

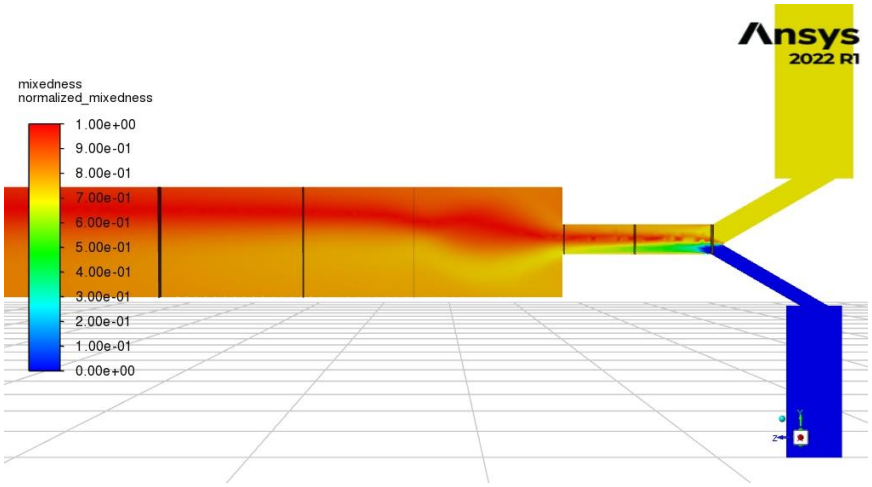

Figure B.12.3: Injector center plane contours of ξ for Run 12c (Small Slot, ϕ = 1.5 with increased back pressure).

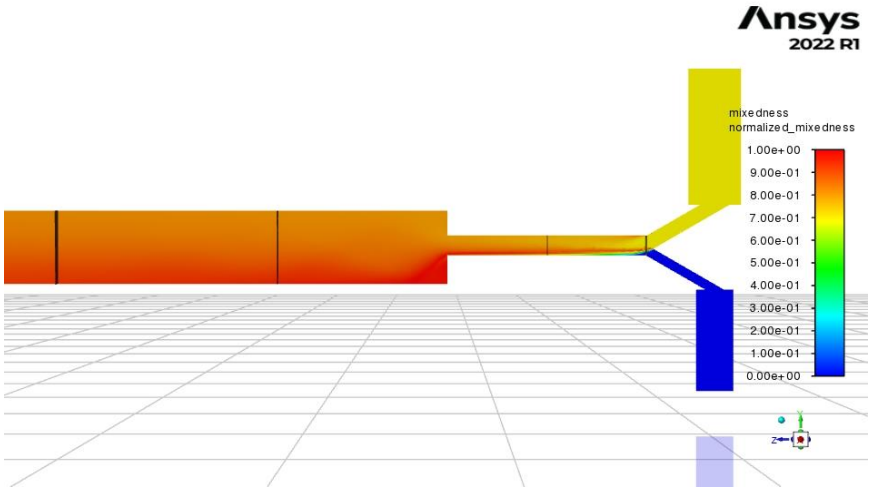

Figure B.13: Injector center plane contours of ξ for Run 14(Large Slot, ϕ = .5).

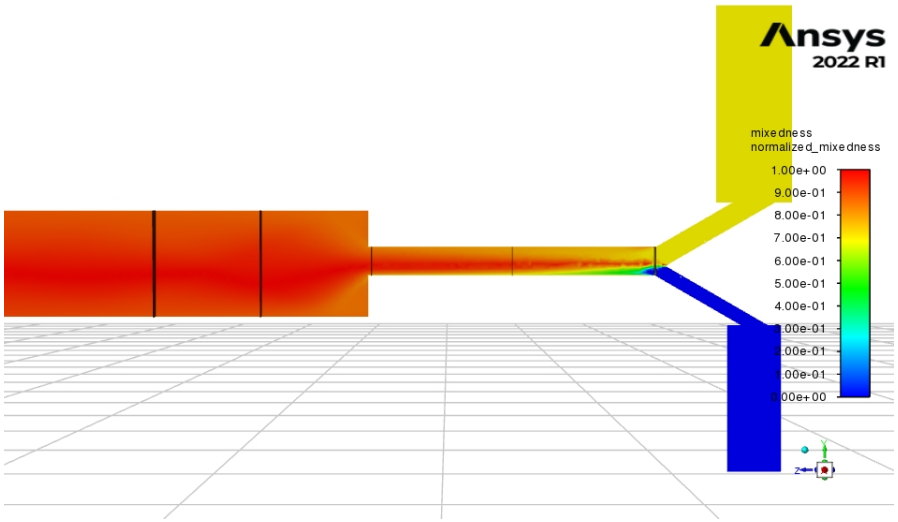

Figure B.14: Injector center plane contours of ξ for Run 13(Large Slot, ϕ = 1).

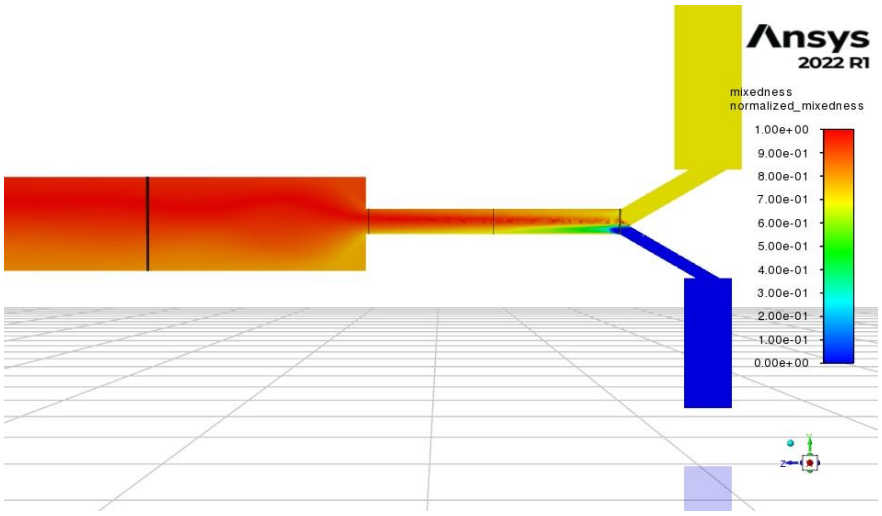

Figure B.15: Injector center plane contours of ξ for Run 15(Large Slot, ϕ = 1.5).

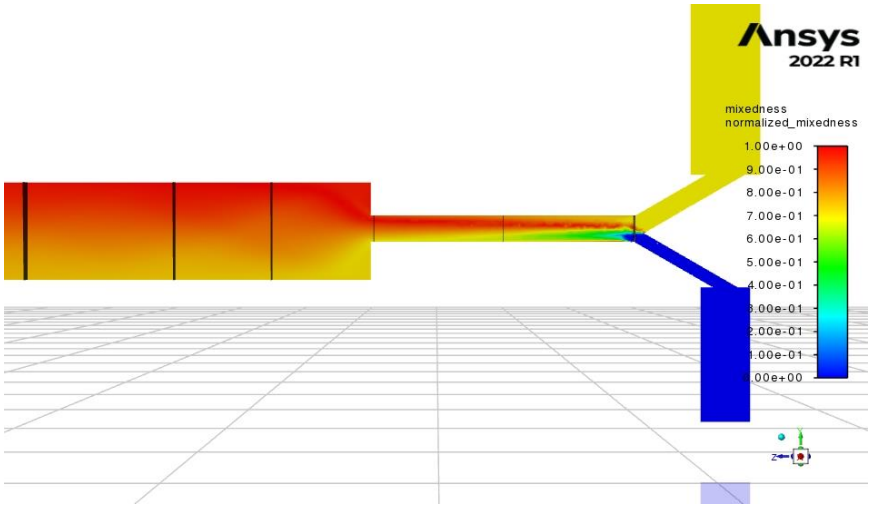

Figure B.16: Injector center plane contours of ξ for Run 16(Large Slot, ϕ = 2).

APPENDIX C:

Mixedness Axial Profile Comparisons

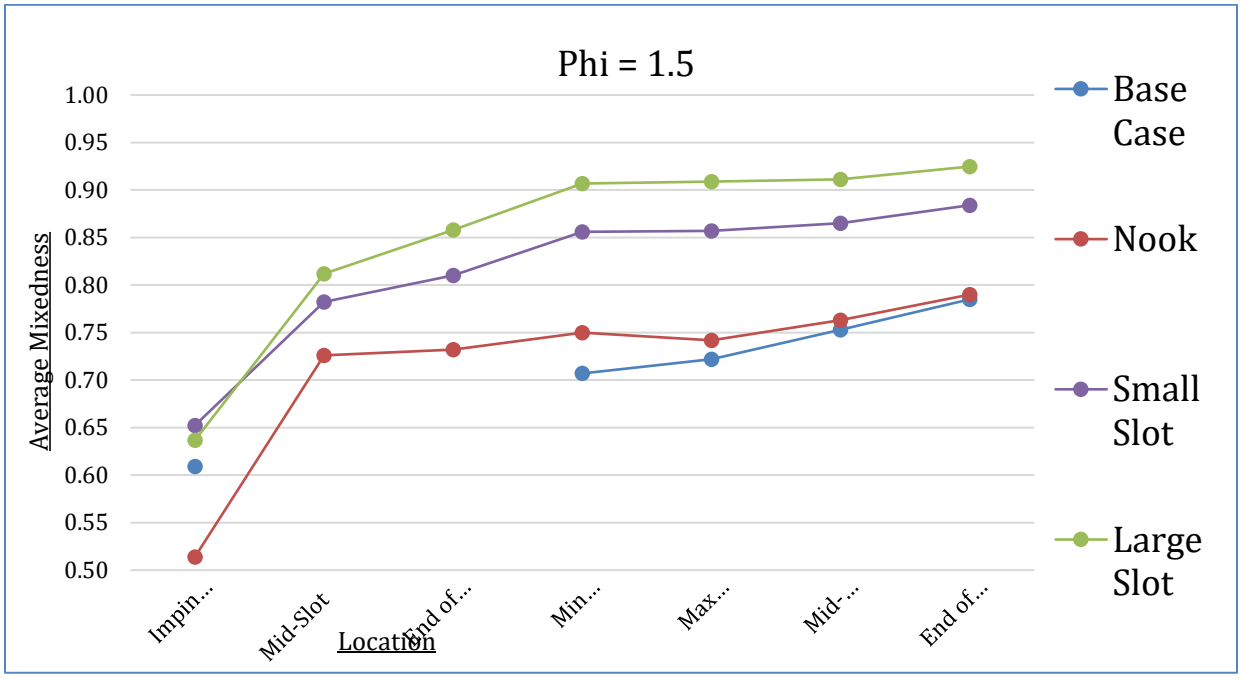

Figure C.1: Planar mixedness averages across geometries for ϕ=1.5

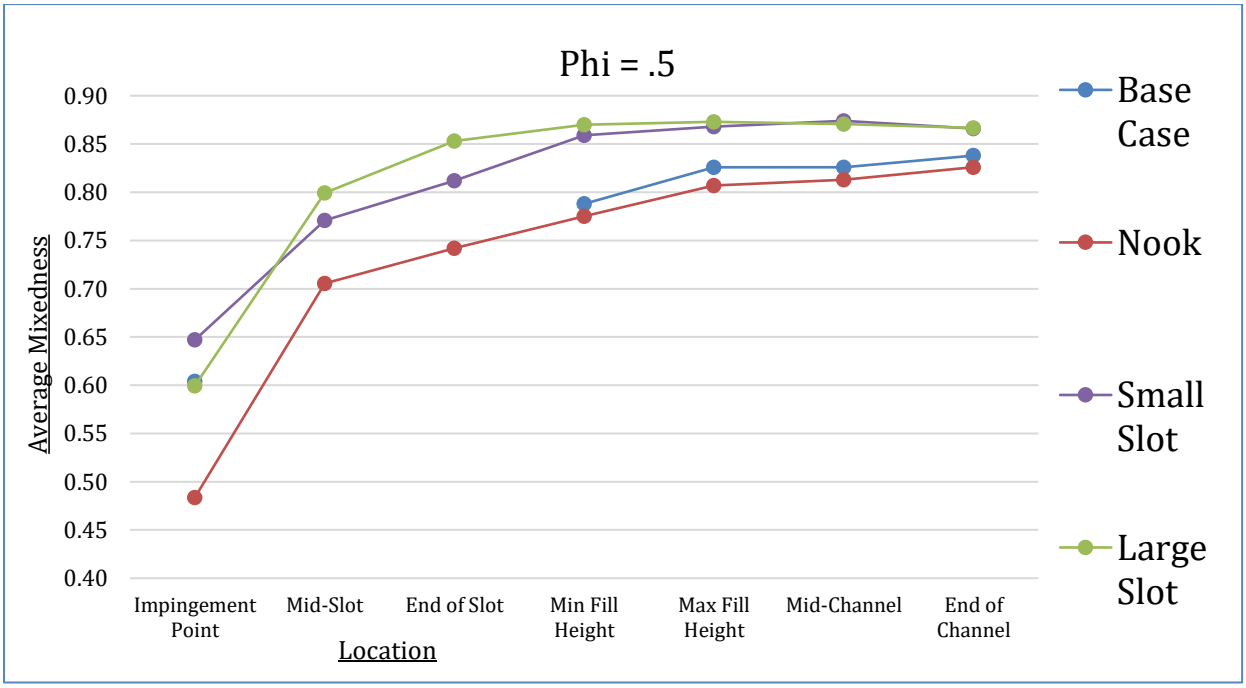

Figure C.2: Planar mixedness averages across geometries for ϕ=.5

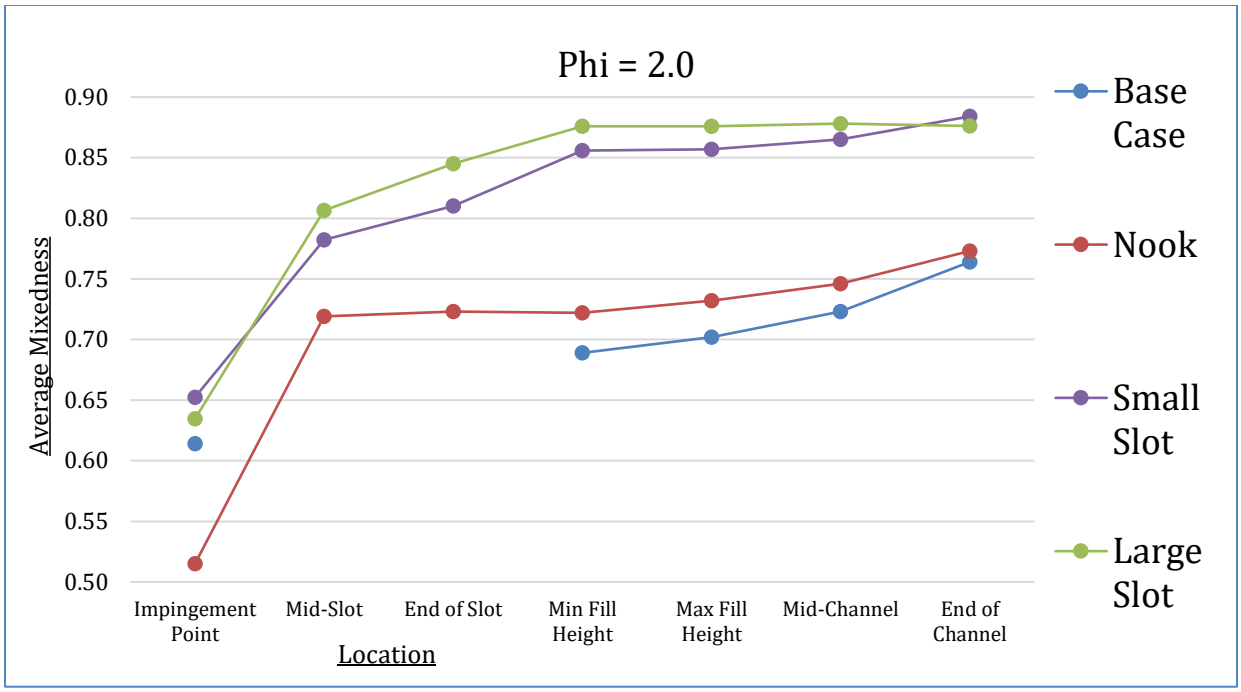

Figure C.3: Planar mixedness averages across geometries for ϕ=2

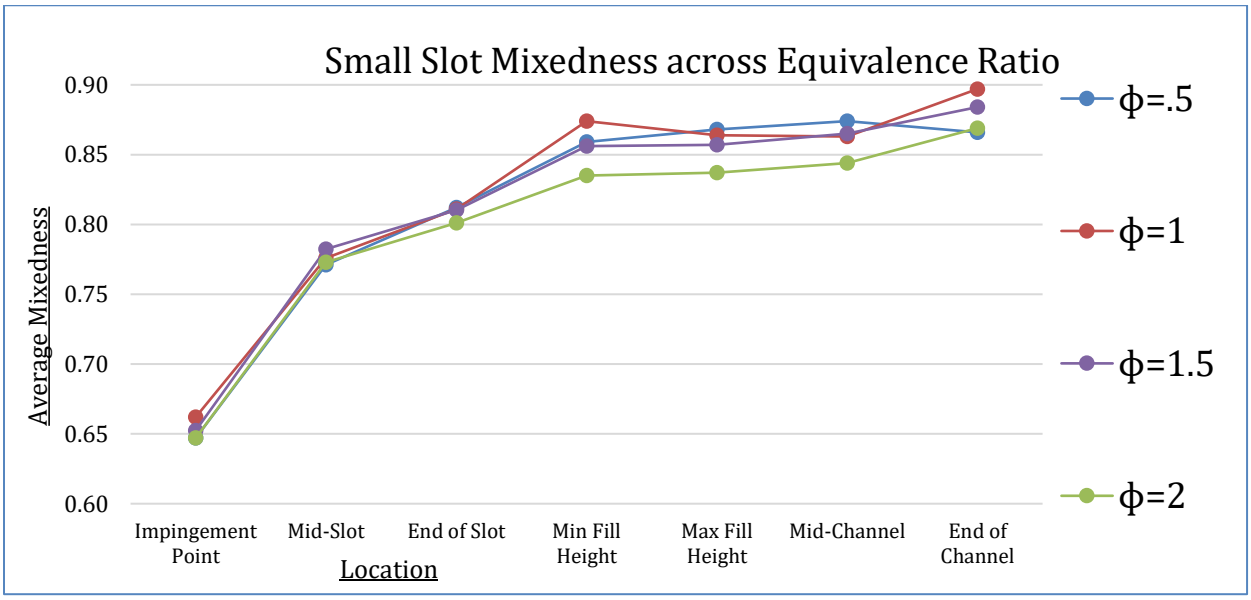

Figure C.4: Planar mixedness averages across all ϕ for small slot geometries